Does the lava lake of Erta 'Ale volcano respond to regional magmatic and tectonic events? An investigation using Earth Observation data

T. D. BARNIE[1,2]*, C. OPPENHEIMER[2] & C. PAGLI[3]

[1]*Department of Geography, University of Cambridge, Downing Place, Cambridge CB2 3EN, UK*

[2]*Present address: Department of Physical Sciences, The Open University, Walton Hall, Milton Keynes MK7 6AA, UK*

[3]*Dipartimento di Scienze della Terra, Università di Pisa, Via S. Maria 53, 56126 Pisa, Italy*

**Corresponding author (e-mail: talfan.barnie@open.ac.uk)*

Abstract: Erta 'Ale volcano lies at the centre of the Erta 'Ale rift segment in northern Afar, Ethiopia and hosts one of the few persistent lava lakes found on Earth in its summit caldera. Previous studies have reported anecdotal evidence of a correlation between lake activity and magmatic and tectonic events in the broader region. We investigated this hypothesis for the period 2000–15 by comparing a catalogue of regional events with changes in lake activity reconstructed from Earth Observation data. The lava lake underwent dramatic changes during the study period, exhibiting an overall rise in height with concomitant changes in geometry consistent with a change in heat energy balance. Numerous paroxysms occurred in the lake and in the north pit; a significant dyke intrusion with subsequent re-intrusions indicated a role for dykes in maintaining the lake. However, despite some coincidences between the paroxysms and regional events, we did not find any statistically significant relationship between the two on a timescale of days to weeks. Nevertheless, changes in lake activity have preceded the broad increase in regional activity since 2005 and we cannot rule out a relationship on a decadal scale.

The Erta 'Ale lava lake lies in the centre of the Erta 'Ale axial volcanic range, an 80 km long by *c.* 30 km wide ridge of aligned and coalesced volcanic centres at the northern end of the Red Sea rift system within the Afar Depression, Ethiopia (Barberi & Varet 1970; Barberi *et al.* 1970; see Fig. 1a). The lava lake lies at the summit of Erta 'Ale volcano, from which the volcanic range gets its name, at 600 m altitude in an elliptical caldera *c.* 1.6 km long by 0.9 km wide (Fig. 1b). The floor of the caldera contains two pits, one *c.* 200 m in diameter at the northern end (the north pit, Fig. 1c) and one *c.* 170 m in diameter in the centre (the south pit, Fig. 1d). The north pit contained a lava lake up to the late 1970s when the pit drained and has subsequently contained fumaroles and occasional spatter cones; the south pit still contains a lava lake today. Up to 2010, the lava lake occupied the southwestern end of the south pit and was bordered by a 'bench' of solid basalt on to which the lake would occasionally overflow.

Persistent lava lakes, such as those at the Erta 'Ale, Nyiragongo, Kīlauea and Erebus volcanoes, are of great interest because they expose the uppermost part of an active magmatic system at the surface. This not only allows direct observations of surface motion, heat loss, gas chemistry and gas flux (e.g. Spampinato *et al.* 2013; Peters *et al.* 2014), but also direct observations of the lake level, which must respond dynamically to pressure in the magma reservoir feeding the lake, the conduit geometry, the magma ascent rate and the amount of degassing (vesiculation), among other factors (Field *et al.* 2012). Observations of lava lakes thereby provide valuable information that helps in understanding volcano dynamics. The effects of external influences such as tides and regional magmatic–tectonic events are of particular interest as they have been hypothesized to have a significant influence on the timing of eruptions (e.g. Darwin 1840; Palmieri 1873; Jaggar *et al.* 1924; Shimozuru 1975, 1987; Neuberg 2000; Hill *et al.* 2002; Manga & Brodsky 2006; Eggert & Walter 2009; Sottili & Palladino 2012).

The history of observations linking earthquakes and volcanic eruptions separated by large distances extends back into the nineteenth century (Darwin 1840). Large earthquakes have been observed to trigger seismic swarms in magmatic regions (e.g. Hill *et al.* 1993) and correlations have been found

From: WRIGHT, T. J., AYELE, A., FERGUSON, D. J., KIDANE, T. & VYE-BROWN, C. (eds) 2016. *Magmatic Rifting and Active Volcanism*. Geological Society, London, Special Publications, **420**, 181–208.
First published online March 30, 2016, http://doi.org/10.1144/SP420.15

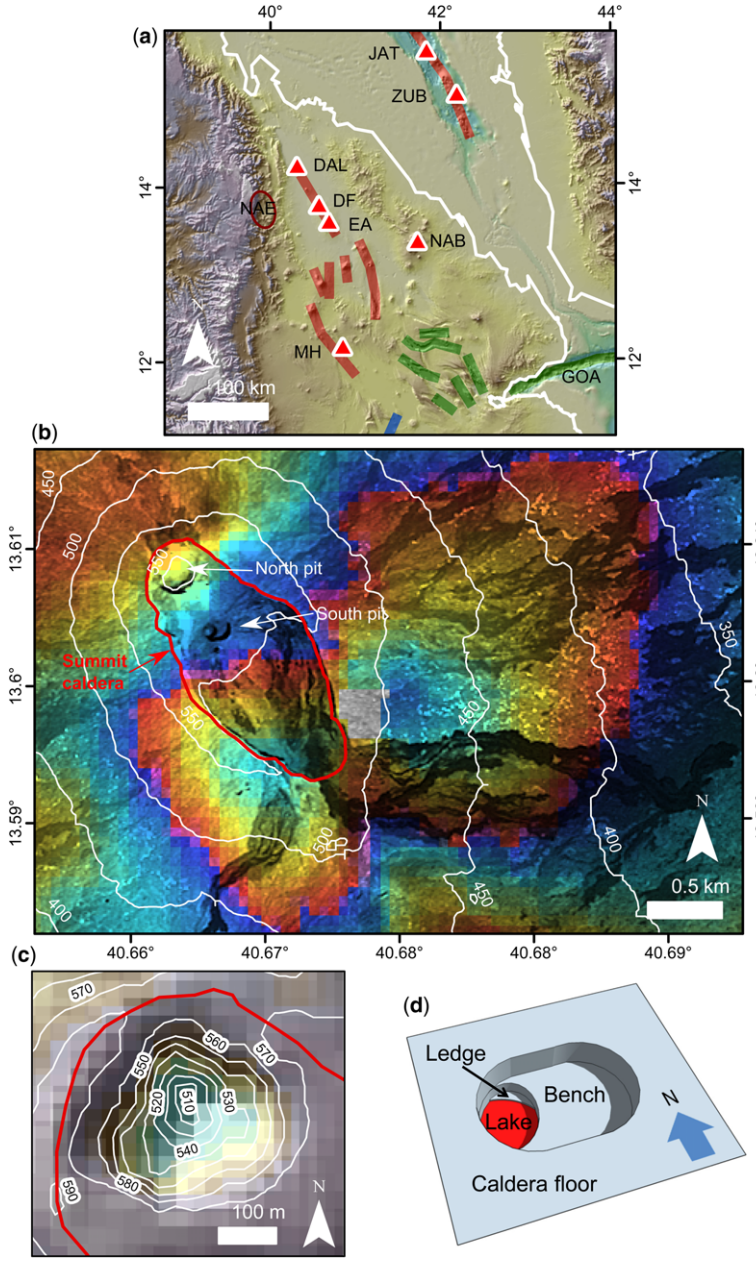

Fig. 1. (**a**) Map showing the location of the Erta ‘Ale lava lake and all the regional magmatic and tectonic events used in this study. DAL, Dallol dyke; DF, Dalaffilla; EA, Erta ‘Ale; GOA, Gulf of Aden; JAT, Jebel al Tair; MH, Manda Hararo; NAB, Nabro; NAE, North Afar Earthquakes; ZUB, Zubair. (**b**) Interferogram of the Erta ‘Ale summit area for epoch 2 January 2004 to 6 May 2004, pan-sharpened using a panchromatic ALI image. A lava lake is currently hosted in the south pit, but one was also present in the north pit until the 1980s. Caldera rim outlined in red, height contours in white. (**c**) Hill shade SRTM 30 m digital elevation model of the north pit showing the topography in February 2000 at the start of the study period. The north pit was extensively infilled with lava over the following 15 years. (**d**) Simple geometric model of the configuration of the south pit from late 2005 until 2010. The lava lake occupied the southwestern corner of the pit floor. The rest of the pit floor formed a flat bench, with a small arcuate ledge on the northeastern flank of the lake sometimes visible. The relative height of the lake with respect to the bench can be judged by the amount of shadowing visible on its eastern side.

between earthquakes and volcanism across a range of geographical and tectonic settings (Eggert & Walter 2009). Searches of global catalogues of volcanic eruptions and large earthquakes separated by hundreds of kilometres have identified more volcanic eruptions than expected within a day or two of large magnitude earthquakes (Linde & Sacks 1998; Manga & Brodsky 2006; Eggert & Walter 2009). Earthquakes are thought to trigger magmatic activity either by changes in static stress due to the displacement of the crust or changes in short-term stresses induced by the passing seismic waves (Hill *et al.* 2002; Manga & Brodsky 2006). The former decay rapidly to below the level of tidal stresses with distance from the epicentre and so are probably too weak to trigger magmatic activity in all but the closest locations (e.g. La Femina *et al.* 2004), so the passage of seismic waves is thought to account for most of the observed triggering. Several mechanisms have been proposed, including rectified diffusion, advective overpressure, increased bubble nucleation, hydraulic surges and destabilization of the crystallized layers in magma chambers. For summaries of statistical studies and an overview of these hypotheses, see Hill *et al.* (2002), Manga & Brodsky (2006) and Eggert & Walter (2009). There is evidence that open vent or frequently erupting volcanoes are less susceptible to seismic triggering than infrequently erupting volcanoes (Walter 2007; Walter & Amelung 2007; Eggert & Walter 2009).

In the case of the Erta 'Ale lava lake, several external triggers have been proposed. Ayele *et al.* (2007*a*) identified an increase in infrared radiation from the lava lake that coincided with the onset of the Manda Hararo rifting event, a rift cycle that consisted of the intrusion of 14 dykes between 2005 and 2012, associated with a small rhyolitic eruption and two large fissure eruptions (Wright *et al.* 2006; Grandin *et al.* 2009; Ebinger *et al.* 2010). Ayele *et al.* (2007*a*) hypothesized that changes in the regional stress field associated with the intrusion of the September 2005 dyke were responsible for the change in behaviour of the lava lake about 150 km to the north. Field *et al.* (2012) noted that the 2010 Erta 'Ale overflows coincided with a major magmatic–tectonic event in the Gulf of Aden. It has also been noted that the broader region is currently experiencing an upsurge in magmatic and tectonic events (e.g. Goitom *et al.* 2015; Jónsson & Xu 2015). We integrated a variety of Earth Observation datasets across a range of spatial and temporal scales to reconstruct changes in the behaviour of the lake over the past decade, extending the work of Oppenheimer & Francis (1997), Wright & Pilger (2008), Field *et al.* (2012) and Murphy *et al.* (2013). We then compared this record with that of the magmatic–tectonic events to investigate the influence of potential external forcings. In the following sections, we first review observations of the lava lake up to 2014 and then consider the spaceborne sensors suitable for reconstructing changes in lake activity.

Review of prior observations of Erta 'Ale

The Erta 'Ale range lies in northern Afar, Ethiopia and forms part of the Red Sea rift system, which steps right-laterally on to the African continent from the Red Sea itself (Barberi *et al.* 1972; Hayward & Ebinger 1996). The range is a rift segment transitional between continental rifting and seafloor spreading (Hayward & Ebinger 1996).

As a result of the logistical difficulties in accessing the site, direct observations of activity have been sporadic. Observations of a glow at the summit of the volcano were first recorded by travellers from 1906 onwards and lava lakes, fresh lava flows and fumaroles visible from the air were reported from the 1940s (Mohr 1962; Barberi & Varet 1970; Varet 1971).

The first regular ground observations were made by a series of joint Franco-Italian CNR/CNRS field campaigns between 1968 and 1973, during which lava lakes were found in both the north and south pits. The lake levels rose over this period such that the rim of the south pit was built up by *c.* 8 m, the floor of the caldera was raised *c.* 4 m and the northern rim of the caldera was breached by lava flows that descended the flanks (Varet 1971; Barberi *et al.* 1973; Tazieff 1973; Le Guern *et al.* 1979). Le Guern *et al.* (1979) used thermometry to estimate the power output from the lava lake to be about 230 MW.

After the CNR/CNRS field campaigns, there was no scientific expedition to the lava lake until the 1990s. To plug the gap, Oppenheimer & Francis (1997) gathered a range of satellite observations from Landsat, JERS-1, SPOT and Advanced Very High Resolution Radiometer (AVHRR), which provided three useful pieces of information: (1) the areal extent of overflows; (2) the depth of the lava lake from shadowing; and (3) the thermal power output. They found no significant overflow between March 1975 and June 1997; shadowing within the pit indicated that the lake level in the central pit remained *c.* 100 m below the rim from at least 1984 to 1997. Thermal observations in the 1980s and 1990s indicated the presence of a lava lake in the south pit and the solidification of the northern lake, with a convective and radiant power output of 100–400 MW. Oppenheimer & Francis (1997) interpreted the apparent steady state of the southern lava lake to indicate that either the caldera floor effectively 'floats' on a shallow magma body or that cooling, crystallization and degassing are evenly matched with the input of fresh magma.

Field visits resumed in the early to mid-1990s and field observations between 1992 and 1995 confirmed the depth of the lava lake in the south pit to be between 90 and 100 m (Oppenheimer & Francis 1998). Harris *et al.* (1999) tried a different approach using satellite infrared remote sensing, choosing to model the lava lake to be composed of crust and/or fresh hot material surrounded by material with a uniform ambient temperature within a given pixel. From this model they estimated the surface temperatures and therefore the convective and radiative heat losses, from which they then estimated magma supply rates of 44–104 kg s^{-1}. Both Harris *et al.* (1999) and Oppenheimer & Francis (1998) noted the importance of endogenous growth of the volcanic edifice, given the sustained lava lake activity, conduit bi-flow and lack of overflows.

Since ground visits resumed in the 1990s, and with the proliferation of orbital sensors, there has been a resurgence in interest in the lava lake, both as a case study of an exposed subaerial magma system and as a terrestrial analogue for features found elsewhere in the solar system (Davies *et al.* 2011). Orbital remote sensing provides a useful first-order continuous overview of trends in activity at the summit; this has taken the form of high temporal resolution thermal observations from low Earth orbit meteorological satellite instruments such as the MODerate resolution Imaging Spectrometer (MODIS) and ground deformation measurements derived from Interferometric Synthetic Aperture Radar (InSAR) techniques. Amelung *et al.* (2000) noted that there was very little deformation along the range between June 1993 and May 1996, with the exception of localized subsidence at Gada 'Ale in the far north of the Erta 'Ale range. The first major deformation observed was associated with the large Dalafilla eruption that occurred north of the lava lake in 2008 (Pagli *et al.* 2012). Wright & Pilger (2008) estimated the heat flux from Erta 'Ale using MODIS satellite images from early 2001 to late 2006 and found a period of high power output (up to *c.* 100 MW) from early 2001 to late 2002, low power output in 2003 (up to 20 MW), a small increase in 2004 (up to 40 MW), quiescence (no detectable radiation) in the last quarter of 2004 and first quarter of 2005, steadily increasing during 2005 and remaining roughly constant through 2006 (up to 60 MW), with a large spike in 2006 (up to 110–120 MW). Ayele *et al.* (2007*a*) examined the period from late 2005 to the beginning of 2006 in more detail and linked an increase in radiant heat from the lava lake with the onset of the Manda Harraro rifting event, hypothesizing that changes in the regional stress field associated with the intrusion of the September 2005 megadyke were manifested in lava lake activity.

Occasional field observations since 1990 have helped to constrain the remote sensing observations. In the 1990s and early 2000s, the lake level appears to have been consistently around 70–100 m below the pit rim (Global Volcanism Program 1992; Burgi *et al.* 2002; Harris *et al.* 2005). Between March 2003 and December 2004, the lake shrank until it was completely frozen over, with four hornitos marking points of degassing (Global Volcanism Program 2004*a*, *b*; Oppenheimer *et al.* 2004), consistent with the MODIS observations of Wright & Pilger (2008). The lava lake reactivated in March 2005; during the period 1–2 September 2009 the lake was reported to be 55 m in diameter, 30 m below the crater rim and gently overturning with frequent 2–3 m high fountains (Davies *et al.* 2011); by 8 February 2010 the lake was 65 m wide and 20 m below the crater rim (Global Volcanism Program 2010).

Thermal observations of the lava lake, whether by optical pyrometer (e.g. Burgi *et al.* 2002) or various types of infrared camera (Oppenheimer & Yirgu 2002; Spampinato *et al.* 2008), typically show the same evolutionary pattern of the lava lake surface, with new crust being created at incandescent cracks and moving away from the cracks as semi-rigid plates to the lake edge where cold crust is subducted. The incandescent material is typically 700–1100°C and the cooler crust is 300–600°C (Oppenheimer & Yirgu 2002; Oppenheimer *et al.* 2004; Spampinato *et al.* 2008), although Davies *et al.* (2011) measured peak temperatures of around 1150°C. The crust migrates across the lava lake at speeds between 0.01 and 0.4 m s^{-1}, cycling between periods of faster and slower motion on a timescale of tens to hundreds of minutes (Harris *et al.* 2005; Spampinato *et al.* 2008). The cycle starts with the rupture and subduction of old crust around the perimeter and new crust forms in the cracks. The lake is eventually completely resurfaced with new crust that becomes jammed, halting motion until the cycle starts again (Oppenheimer *et al.* 2004). The lake has been observed in a completely crusted state, when lava and gas emissions are typically limited to a few hornitos (Global Volcanism Program 2004*a*).

The resurfacing cycles vary in magnitude. Oppenheimer *et al.* (2004) observed cyclic variations in radiative power output between 10 and 25 MW over a full cycle in March 2003, whereas (Spampinato *et al.* 2008) observed cycles varying between 45 and 76 MW in November 2006. The variation in power output with surface speed reflects the interplay between the surface heat loss, the exposure of incandescent material and the resurfacing rate (Harris *et al.* 2005). These power outputs have been used to estimate magma supply rates of 500–600 kg s^{-1} (Burgi *et al.* 2002), although all

such calculations are based on 'guesstimates' of the key parameters (the enthalpy change in magma rising into and sinking from the lake). Harris *et al.* (2005) proposed two models to explain the variation in convection rate: either changes in volume flux and rheology, or convective instabilities. Harris (2008) modelled cooling and crystallization and found that convection can be driven by small (*c.* 6 kg m^{-3}) density differences, which could, in turn, be driven by surface cooling.

In addition, hotspots appear in cracks or in the middle of plates and are associated with mild explosive activity, which is interpreted as the episodic release of over-pressurized gas bubbles at the lake surface (Spampinato *et al.* 2008). Bouche *et al.* (2010) combined detailed video observations of bursting gas bubbles at the surface with acoustic measurements. They observed that hotspots form when bubbles break the surface, and that these are often followed by a trail of smaller bubbles that form fire fountains, with a return period of *c.* 1 h. Bouche *et al.* (2010) attributed the bubble trails to the low Reynolds number of a large spherical cap bubble, which resulted in instability. If the tail separates from the main bubble at shallow depths, then this explains the timing of major bubble bursts and the succeeding fire fountains. Seismic signals from multiple processes in different source regions have been identified, including conduit resonance, bubble bursting and fumarole degassing (Jones *et al.* 2012). Two main sites with a convection cycle have been identified, one located at the northern edge of the lake, the other 100–150 m ENE. These sites may represent two discrete sources, or a variety of processes that interfere with each other as they wax and wane over a cycle.

Gas measurements at the lava lake have been limited. Oppenheimer *et al.* (2004) measured the SO_2 flux from the lake in March 2003 as *c.* 0.7 kg s^{-1}, equivalent to a magma mass flux of 350–650 kg s^{-1}. On 15 October 2005, following the onset of the Manda Hararo event, Sawyer *et al.* (2008) measured an average SO_2 flux of 0.69 $\pm$ 0.17 kg s^{-1} using ultraviolet spectrometry and found significant increases in the proportion of H_2O with respect to CO_2 and SO_2 compared with observations made in the 1970s (Gerlach 1980), which they attributed to either the depletion of volatiles during effusive eruptions in the 1970s or fractional degassing between the two pit craters.

There have been very few attempts to measure the physical properties of the lava. Burgi *et al.* (2002) measured the radiant temperature of various points on the lake surface with a pyrometer and estimated the emissivity by comparing these observations with temperatures derived from a thermocouple attached to a metal plate in contact with the lava surface, retrieving an emissivity of 0.74. This value is very low compared with that estimated from laboratory measurements and the values typically assumed in the remote sensing literature (0.95–1.0) (e.g. Ball & Pinkerton 2006).

In summary, there appears to have been persistent activity at the summit since at least the beginning of the twentieth century, with local oral traditions suggesting a much longer history of activity. The period 1969–73 witnessed a rise in the level of the lava lake, whereas that from about 1974 to 2003 saw a fairly stable lava lake level. The lake area contracted between 2003 and 2004, at one point freezing over almost completely. The onset of the Manda Hararo rifting cycle in 2005 appears to coincide with a rejuvenation of the lava lake and the geometry of the lake within the pit remained roughly in the configuration shown in Figure 1d until the overflows of 2010. The lake activity consists of a cycle of plate production at incandescent cracks and subduction at the lake margins at varying speeds over a timescale of 10–100 min, with periodic large bubble bursts followed by fire fountains associated with trailing small bubbles occurring over timescales of *c.* 60 min.

Methods

In this study, we tracked changes in activity at Erta 'Ale volcano using Earth Observation data. Our ability to track changes in volcanic activity using satellite images is limited by a series of trade-offs between spatial resolution, spectral resolution, dynamic range, acquisition frequency and the volume of data. We were able to overcome some of these limitations by jointly interpreting observations from a range of instruments (e.g. Murphy *et al.* 2013). We were able to (1) identify changes in geometry at small spatial scales, (2) discriminate between thermal emissions from closely spaced sources and (3) identify high-frequency events, all while maintaining a synoptic view over long time periods. To facilitate this, we developed a series of indices and measurements derived from images acquired by a number of instruments to track changes in (1) the radiative output of the north pit and the lava lake, (2) gas emissions from the north pit, (3) changes in the geometry of the lava lake and the surrounding south pit and (4) ground deformation.

The optical satellite data used in this study can be grouped into two classes: moderate resolution or 'Landsat-like' (Powell *et al.* 2007) data with spatial resolutions in the tens of metres and repeat times measured in days to weeks; and low resolution weather satellites with resolutions in kilometres and repeat times in minutes to hours. The Landsat-like instruments used were the Advanced Land

Imager (ALI) aboard NASA's Earth Observing 1 (EO-1) satellite, which was launched in November 2000 (Ungar *et al.* 2003) and the Enhanced Thematic Mapper Plus (ETM+) aboard NASA's Landsat 7 satellite, launched in April 1999 (Goward *et al.* 2001). Both these instruments acquire images from the visible to the short wave infrared (SWIR) region at 30 m resolution. In addition, ALI and ETM+ acquire a panchromatic band at 10 and 15 m, respectively, and ETM+ acquires a thermal infrared (TIR) band at 60 m. The Landsat 7 data were subject to failure of the scan line corrector (SLC) after 31 May 2003, resulting in missing data in horizontal bands across the image (Markham *et al.* 2004), the impact of which is discussed in the results section. All datasets were ordered from the USGS Earth Explorer website at level 1T (precision- and terrain-corrected) for daytime images and level 1GST (precision-corrected) for night-time images. Level 1GST images are less accurately georeferenced and sometimes need to be manually aligned with better constrained datasets. Data from these instruments have been extensively used for volcanological studies (e.g. Flynn *et al.* 2001; Donegan & Flynn 2004) and ALI is frequently tasked to acquire images of volcanoes as part of the Autonomous Sensor Experiment (Davies *et al.* 2006).

The low resolution weather satellite class consists of the MODIS aboard NASA's Low Earth Orbit Terra and Aqua satellites and the Spinning Enhanced Visible and Infrared Imager (SEVIRI) on board EUMETSATS's geostationary Meteosat Second Generation family of satellites. The MODIS instruments typically acquire four images of a target each day at 1 km resolution in the TIR at nadir (Justice *et al.* 1998, 2002); however, in this study we used an operationally produced fire data product and did not process the images ourselves. The SEVIRI instrument acquires images of the full Earth disc in 12 bands every 15 minutes (Aminou *et al.* 1997; Aminou 2002). Pixel spacing at the sub-satellite point is 3 km for the TIR bands of interest, increasing towards the image margins as a result of the curvature of the Earth. Images are acquired using a whisk-broom principle: three detectors offset vertically are scanned across the Earth's surface as the satellite spins and are progressively stepped north. The archive of images extends back to early 2004. In this study, we used band 4 (3.9 μm) images, processed to level 1.5 (radiometrically and geometrically corrected; Müller 2010) and converted to radiance in units of $W\,m^{-2}\,sr^{-1}\,\mu m^{-1}$. Both MODIS and SEVIRI are widely used for volcanological studies (e.g. Wright *et al.* 2004; Ganci *et al.* 2011).

Finally, we used synthetic aperture radar images acquired by the European Satellite ENVISAT to generate interferograms and measure ground deformation in the satellite line of sight. The aforementioned datasets were used to derive measurements and indices to track activity at Erta 'Ale.

MODIS Fire Radiative Power data

We used the MCD14ML Global Monthly Fire Location product, collection 5.1 (Giglio 2013), as distributed by the Fire Information for Resource Management System (FIRMS; Davies *et al.* 2009), to track the total power output of the combined north pit and lava lake. This data product is an ASCII text list of fire pixels, specifying their location and fire radiative power (FRP) in megawatts (MW) per pixel. The fire pixels were detected in MODIS images using a series of absolute and relative brightness temperature thresholds (Giglio *et al.* 2003) with the FRP calculated using an empirical relationship derived from models of fires with varying proportions of smouldering and flaming phases (Kaufman *et al.* 1998); for an overview, see Justice *et al.* (2006). The FRP record for Terra MODIS data extends back to November 2000, whereas that for Aqua extends back to August 2002.

The FRP is calculated using a model of wildfires that obviously does not apply to lava lakes; however, we were mainly interested in using the FRP to study the variability in lake activity and, in particular, to identify periods of increased lake activity, rather than using the absolute values to derive a physical parameter (e.g. mass flux). In this study, we selected all the fire pixels within a window surrounding the Erta 'Ale summit caldera. The surface within the selection window consists of unvegetated old basalt flows and there is no strong contrast in surface type (e.g. between the basalt and the surrounding desert), so we are confident that the time-series does not contain many wildfires or false positives. We summed the FRP from all hotspots acquired at a particular date and time to give a time-series of the total FRP output from the Erta 'Ale caldera region. The low resolution of the sensor does not allow the discrimination of thermal emissions from the lava lake or the north pit.

SEVIRI thermal anomaly

We used SEVIRI to track thermal emissions from the lava lake and north pit at a high temporal resolution. Given the large volume of data acquired by SEVIRI over the lava lake, and the higher sensitivity of MODIS to thermal anomalies due to its smaller pixel size and more favourable look angles, we acquired SEVIRI data only for periods of anomalously high FIRMS power output. We extracted the band 4 (3.9 μm) thermal anomaly signal from this radiance data using the independent component analysis technique of Barnie & Oppenheimer

(2015*b*) applied to the whole image time-series using a 5×5 pixel window centred on the summit and 25 retained principal components. As with MODIS, the resolution of the instrument is insufficient to discriminate between thermal emissions from the lava lake and north pit. Where a sequence of short period events such as lava lake overflows could be identified, we treated the time-series as a 'spike train' and (1) manually identified the onset time or time of maximum radiance for each event, (2) calculated the time intervals in hours between successive events and (3) plotted the interspike interval (ISI) histogram to identify the dominant period.

North pit thermal infrared (TIR) anomaly

We isolated thermal emissions from the north pit using the moderate resolution TIR band of ETM+ (band 6, low gain mode, 10.40–12.50 μm, 60 m resolution, interpolated to 30 m in the final data product) and calculated the anomaly by subtracting the average from a neighbouring background region on the flank of the volcano from the mean at sensor radiance within the pit. Assuming that the atmosphere and surface properties vary little spatially, this should subtract out the atmospheric emission and seasonal variation in surface temperature, giving the excess radiance multiplied by the atmospheric transmission. Images with cloud contamination over the north pit or background region were identified manually and removed. The north pit was frequently partially obscured by fumarole emissions prior to 2009; however, these were weak and their effect on the TIR bands is likely to be minimal.

All the ETM+ images were processed identically, except that missing pixels in ETM+ SLC-off images were excluded from the mean radiance calculation. We used the TIR band to calculate the excess thermal radiance instead of the SWIR because this wavelength interval is more sensitive to lower temperatures and therefore more responsive to the residual heat from older eruptions (Davies *et al.* 2010), decreasing the likelihood of missing an emission event. In other words, the TIR and SWIR radiance time-series can be considered to be a convolution of the effusion rate with some cooling kernel (e.g. Davies 1996; Barnie & Oppenheimer 2015*a*), which decays more slowly in the TIR than the SWIR. This results in a smoother curve in the TIR, the shape of which can be adequately captured in fewer observations, mitigating the low rate of acquisition of the Landsat class images. The TIR is also capable of picking up more subtle variations in surface temperature – for example, due to shallow bodies of lava/magma – whereas the SWIR is only sensitive to freshly emitted material at high temperatures. However, the TIR bands typically have a low spatial resolution, so we used fortuitous SWIR observations, where available, to visually investigate the position and extent of smaller thermal anomalies within the pit. We used similar bands in the SWIR and NIR in ETM+ and ALI to make the images comparable; bands 7, 5 and 4p (2.08–2.35, 1.55–1.75 and 0.845–0.89 μm) from ALI and 7, 5 and 4 (2.09–2.35, 1.55–1.75 and 0.77–0.90 μm) from ETM + .

Index of fumarolic activity at the north pit

Estimating fluxes of fumarole emissions from the north pit using Earth Observation data is difficult as a result of (1) a lack of sensors with bands covering absorption features of sufficient sensitivity and resolution to detect the weak emissions of volcanic gas species and (2) insufficient acquisition frequency to ascertain plume speeds. We therefore opted to track fumarole emissions by measuring the presence of highly reflective condensed fumarole plumes over the darker basalt surface. The amount of condensation present (in addition to atmospheric characteristics such as dust) will be a function of the daily and seasonal variation in humidity and wind speed, in addition to the composition and flux of fumarole gases. However, we assumed that both the broad trends and sudden changes between different regimes over the 15-year study period were more likely to be a function of fumarolic than climatic variations.

Identifying variations in condensation was complicated by the resurfacing of the north pit by fresh basalt flows, which resulted in changing reflectance and variation in thermal emissions, as well as variations in reflectance with illumination and view angles, all of which contributed to the variability in sensor radiance. We used top of atmosphere reflectances calculated according to Chander *et al.* (2009) to try to correct for illumination angle effects. Inspection of high-resolution panchromatic images indicated that the reflectance was highly variable within the pit during periods of abundant condensation and the amount of condensation varies from one image to the next, whereas during periods with little condensation the interior radiance of the pit was less variable and fairly constant between images. We therefore opted to estimate the presence of a condensed plume by taking the standard deviation of reflectances within the north pit.

Periods with a wide range of standard deviations are likely to be a function of condensation, whereas persistent low values are likely to be extended periods of little condensation; lava resurfacing is expected to manifest as a trend over time. We used 30 m bands in the visible region to avoid accidentally recording thermal anomalies and to make

the images from both sensors comparable: band 1 (0.45–0.52 μm) in ETM+ and band 1 (0.45–0.515 μm) in ALI. In addition to this quantitative approach, we used high-resolution panchromatic bands to qualitatively assess the presence or absence of condensation.

South pit lake and bench heights

We estimated the depth of the bench below the eastern rim of the south pit and the lake below the bench from shadowing in ETM+ and ALI panchromatic bands. Digitizing the shadow length involves an element of judgement given the low resolution of the images used (10 m for ALI, 15 m for ETM+) and the high level of noise in ETM+ images; we estimated that it was usually possible to digitize the shadow to within ± 0.5 pixel accuracy. We used level 1T (precision- and terrain-corrected) data products for both ETM+ and ALI, which use ground control points for geometric accuracy and digital elevation models (DEMs) for topographic correction. This corrects for large-scale topographic and view angle effects and scales the image to map coordinates. However, the south pit is a small feature and is effectively absent in the DEMs used to correct the ALI and ETM+ images (SRTM-2, 30 m and GLS 2000, 90 m). As a result, for images with off-nadir view angles (which accounts for most of the ALI archive), shadows may be shortened (due to shadow occlusion by the pit rim) or extended (by projecting the shadowed vertical wall onto the horizontal).

We attempted a first-order correction for these effects by modelling the illumination shadow and the view shadow on the bench and correcting the measured illumination shadow for the effects of the view shadow (Fig. 2). In doing so, we made the following assumptions: (1) the level 1T processing corrected for all topographic and scaling effects apart from that due to the pit; (2) the pit has an idealized shape with vertical pit and bench walls and a horizontal bench and lava lake surface; (3) the shadow length is digitized along the illumination path perpendicular to the pit or bench rim; and (4) the curvature of the rim between the Sun shadowing point and the view shadowing point is insignificant (i.e. the angle α in Fig. 2 is a right angle).

We derived the equation for estimating the depth of the bench below the eastern pit rim or the depth of the lake below the bench from the observed shadow and the illumination and view angles. The discussion is given in terms of bench depth, but the same arguments apply for lake depth, which was calculated in the same way. The true length of the illumination shadow on the bench in the illumination direction, s_0, is given by:

$$s_0 = \frac{h}{\tan(\theta_{\text{sun}})} \tag{1}$$

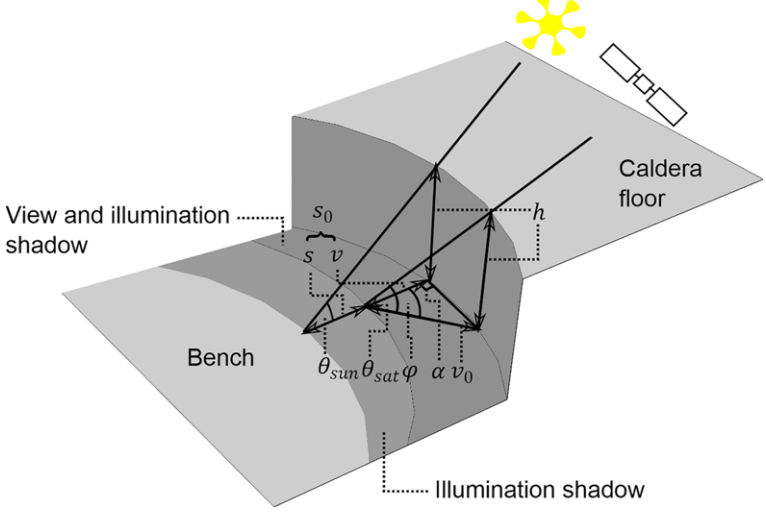

Fig. 2. Diagram showing the view and illumination shadows cast on the bench in the south pit by the Sun and the sensor, together with the variables used to derive the bench height of the vertical wall, h: s_0, true length of the illumination shadow on the bench; θ_{sun}, solar elevation angle; v_0, true length of the view shadow on the bench; θ_{sat}, satellite elevation angle; v, the component of the view shadow in the illumination direction; φ, angle between the solar and view angles; s, observed shadow length in the illumination direction; and α, angle between the horizontal projection of the illumination direction and the line joining the points on the rim casting the illumination and view shadows. The wall height h was calculated using equation (6).

where h is the height of the pit wall and θ_{sun} is the solar elevation angle. Similarly, the true length of the view shadow on the bench, in the view direction, v_0 is given by:

$$v_0 = \frac{h}{\tan(\theta_{sat})} \quad (2)$$

where θ_{sat} is the satellite elevation angle. Negative view shadow lengths indicate that the pit rim is projected onto the bench (some bench shadow is obscured), whereas positive values indicate that the pit rim is projected behind the pit wall (some shadowed pit wall is projected into view). The component of the view shadow in the illumination direction, v is given by:

$$v = v_0 \cos(\varphi) \quad (3)$$

where φ is the angle between the solar and view angles and the observed shadow length in the illumination direction. s is the sum of the true shadow length and v:

$$s = s_0 + v \quad (4)$$

Substituting equations (1) and (3) into equation (4) gives:

$$s = \frac{h}{\tan(\theta_{sun})} + \frac{h}{\tan(\theta_{sat})}\cos(\varphi) \quad (5)$$

Rearranging for h, gives:

$$h = \frac{s}{((1/\tan(\theta_{sun})) - (\cos(\varphi)/\tan(\theta_{sat})))} \quad (6)$$

This gives the bench height in terms of the view and illumination angles and the observed shadow length.

South pit lake area and pit area

The south pit area was found by digitizing the features in ETM+ and ALI panchromatic bands. As before, as a result of the low resolution of both bands and the high noise of the ETM+ panchromatic band, digitizing the pit involved an element of judgement. It was not possible to identify the western end of the pit after the 2010 overflows, so our time-series stops after this point. The lava lake area was digitized from ALI panchromatic images only as the ETM+ images were too coarse and noisy to reliably identify the lake.

InSAR-derived ground deformation

We analysed InSAR data from 2005 to 2010 to reconstruct the time-evolving deformation of the Erta 'Ale volcano. We created 59 interferograms for the InSAR track 049 of the ENVISAT satellite in descending orbit, which offer a long and dense series of acquisitions between 2005 and 2010. We obtained the line-of-sight (LOS) time-series of incremental velocities and displacements using a multi-interferogram method, π-rate software (Wang *et al.* 2012). We used the JPL/Caltech ROI_PAC software (Rosen *et al.* 2004) and a 3 arc second SRTM DEM to create all the interferograms. The data were geocoded to the 3 arc second SRTM DEM (*c.* 90 m resolution) and we then averaged two geocoded neighbouring pixels to *c.* 200 m resolution in all interferograms. The time-series analysis was conducted as described in Pagli *et al.* (2014).

In addition, we identified a sudden deformation signal at Erta 'Ale volcano in an interferogram from track 049, spanning the time period between 2 January 2004 and 6 May 2005. The deformation pattern consists of two lobes of range decrease near the southern edge of the south pit (for location relative to the summit features, see Fig. 1b; the modelled interferogram is shown in Fig. 4). To match the observed deformation, we assumed a shallow dyke (Okada tensile dislocation) in the conventional elastic half-space model, with a Poisson's ratio of 0.25. To estimate the dyke parameters, we applied a formal inversion procedure using a simulated annealing algorithm followed by a derivative-based method (Cervelli *et al.* 2001). For computational convenience, the data size was reduced prior to inversion using quad-tree partitioning, two-dimensional quantization algorithm (e.g. Jónsson *et al.* 2002).

Regional event catalogue

To assess the influence of regional magmatic and tectonic events on activity at the lava lake, we compiled a list of events in the broader Afar–Red Sea–Gulf of Aden–Main Ethiopian Rift region over the duration of the study period (2000–15) by conducting a thorough literature review. The full list of events is given in Table 1 and their locations are shown in Figure 1a. The events are referenced by an acronym, followed by a number where multiple events occurred at the same location.

Results

A summary of all the time-series derived from Earth Observation data, with the exception of the SEVIRI thermal anomaly, is shown in Figure 3. The total radiant power output of the summit caldera region as measured by MODIS FRP is shown in Figure 3a. This time-series reveals the same overall pattern of variation as the MODIS-derived radiant flux reported between 2001 and 2006 by Wright &

Pilger (2008) and the radiance from night-time MODIS images between 2000 and 2012 reported by Murphy *et al.* (2013), despite using a different derived product in this case. Here, we extend the analysis to 2015. In Figure 3a we show only the nadir observations to remove spurious low values due to oblique view angles that occlude some of the hot material, making the sequence less noisy and overall trends easier to identify (the oblique observations are, however, useful for tracking short duration events and the whole dataset is shown in Figs 6 & 7).

The power output was high between the start of 2001 and the end of 2003, low to absent through

Table 1. *Summary of major magmatic–tectonic events in the Afar–Red Sea–Gulf of Aden region between 2000 and 2012*

Label	Event	Start date	Description
NAE	North Afar earthquakes	August 2002	Ayele *et al.* (2007*b*)
EAD	Erta ‘Ale dyke	5 March 2004	Small shallow dyke intrusion at southern tip of northern crater between 2 January 2004 and 6 May 2004; event placed at midpoint of interferogram epoch
DAL	Dallol dyke	22 October 2004	Event placed at onset of seismic swarm. Small dyke and seismic swarm at Dallol *c.* 80 km NNW of Erta ‘Ale (Nobile *et al.* 2012)
MH1	Manda Hararo dyke 1	20 September 2005	8 m wide, 80 km long dyke *c.* 150 km SW of Erta ‘Ale marks onset of Manda Hararo rifting cycle. We place the event at the start of continuous seismic activity on 20 September. All subsequent dykes smaller in scale (Ayele *et al.* 2009)
MH2	Manda Hararo dyke 2	17 June 2006	Event placed at onset of seismic swarm (Keir *et al.* 2009)
MH3	Manda Hararo dyke 3	25 July 2006	Event placed at onset of seismic swarm (Keir *et al.* 2009)
MH4	Manda Hararo dyke 4	10 September 2006	Event placed at onset of seismic swarm (Hamling *et al.* 2009)
MH5	Manda Hararo dyke 5	7 December 2006	Event placed by continuous global positioning system record (Hamling *et al.* 2009)
MH6	Manda Hararo dyke 6	14 January 2007	Event placed by continuous global positioning system record (Hamling *et al.* 2009)
MH7	Manda Hararo dyke 7	11 August 2007	Event placed at onset of seismic swarm (Belachew *et al.* 2011). Dyke associated with fissure eruption (Ferguson *et al.* 2010)
JAT	Jebel al Tair eruption	30 September 2007	Onset of event taken as start of initial paroxysmal fissure eruption, then slow effusion over two to three months, *c.* 250 km NE of Erta ‘Ale (Marchese *et al.* 2009; Xu & Jónsson 2014)
MH8	Manda Hararo dyke 8	11 November 2007	(Hamling *et al.* 2009) reported intrusion began on 12 November from global positioning system data; (Belachew *et al.* 2011) places it on 11 November from seismic data
MH9	Manda Hararo dyke 9	31 March 2008	Event placed at onset of seismic swarm (Belachew *et al.* 2011)
MH10	Manda Hararo dyke 10	9 July 2008	Event placed at onset of seismic swarm (Belachew *et al.* 2011)
MH11	Manda Hararo dyke 11	17 October 2008	Event placed at onset of seismic swarm (Belachew *et al.* 2011)
DF	Dalafilla eruption	3 November 2008	Fissure eruption *c.* 25 km NW of Erta ‘Ale (Pagli *et al.* 2012)
MH12	Manda Hararo dyke 12	11 February 2009	Event placed at onset of seismic swarm (Ebinger *et al.* 2010)
MH13	Manda Hararo dyke 13	28 June 2009	Event placed at onset of seismic swarm (Belachew *et al.* 2011). Dyke associated with fissure eruption at the Manda Hararo rift segment (Ferguson *et al.* 2010)
MH14	Manda Hararo dyke 14	20 May 2010	Event placed at start of seismic swarm. Dyke associated with fissure eruption. See Barnie *et al.* (2015)
GOA	Gulf of Aden dyke	14 November 2010	Event placed at start of seismic swarm. Major rift event, propagating swarm probably indicates intrusion of dykes with >10 m extension (Ahmed *et al.* 2016; Shuler & Nettles 2012)
NAB	Nabro	12 June 2011	Event placed at start of eruption. Explosive/effusive eruption *c.* 120 km from Erta ‘Ale (Hamlyn *et al.* 2014)
ZUB	Zubair	13 December 2011	Event placed at onset of seismicity. Two M3 earthquakes on 13 December 2011, eruption starts by 18 December 2011, initially subaqueous, constructs an island visible in satellite images by 23 December 2011 (Global Volcanism Program 2011*b*)

to the first quarter of 2005, with isolated spikes in 2004, then increased through the remainder of 2005, followed by a long decreasing trend, with some spikes, until mid-2010, and then a long increasing trend until 2015. Unfortunately, it was not possible to separate the thermal emissions from the lava lake and the north pit due to their small spatial separation (*c.* 500 m) and the coarse resolution of MODIS (1 km pixel spacing at nadir).

The north pit TIR anomaly is shown in Figure 3b. There was saturation of some pixels within the pit despite using the low gain TIR band; however, an overall trend is still visible. Between 2000 and 2004 the TIR anomaly was fairly constant and negative, indicating that the north pit was radiating less than the flank of the volcano, perhaps due to shadowing reducing the solar insolation. There was a peak in the anomaly from April to November 2004 (coincident with a period of low background MODIS FRP with isolated spikes), indicating that the pit was radiating substantially more than the flank. The anomaly remained positive thereafter with two more peaks: one peak from March to October 2010 that coincided with another period of isolated peaks in the MODIS FRP and another peak from December 2012 to January 2013.

A series of ETM+ band 6 TIR images used to calculate the anomaly are given below the graph, showing the rough location of the thermal anomalies within the pit during the peaks in radiance. There was no stepwise change in the pattern between the SLC-on and SLC-off ETM+ images, so the SLC fault does not appear to have compromised our results in this instance. During quiescent periods between the peaks in TIR radiance, persistent small anomalies of the order of a few pixels were frequently seen in the SWIR – the numbers of these that were visible in the ETM+ and ALI images are shown in Figure 3c, with example images shown below the graph. These minor anomalies were absent between 2000 and 2004, with one occasionally visible in 2003 and 2004, two present (one roughly in the centre, one at the northern edge) from late 2004 to 2006, after which the northern anomaly disappeared and the central anomaly remained until the end of 2013, after which no SWIR anomaly was present.

The north pit fumarole index is shown in Figure 3d, with values high and variable between 2000 and 2008, declining through 2010, and persistently low afterwards. This pattern is consistent with a decrease in the frequency of the presence of a high albedo condensed fumarole gas component over the pit in the short wavelength visible region, which can be confirmed by visually inspecting the higher resolution panchromatic images shown the plot. The high albedo feature is frequently located over the centre of the pit at the location of the central, small persistent SWIR anomaly identified in Figure 3b. Again, values from the ALI, ETM+ SLC-on and ETM+ SLC-off images overlap one another and appear to follow roughly the same trend, indicating that the results from all three datasets are comparable.

The changing areas of the lava lake and the surrounding south pit are shown in Figure 3e and f, respectively. The overall trend in lake area decreased from *c.* 8000 to *c.* 1000 m^2 between 2000 and late 2010, with an increase to *c.* 3500 m^2 by 2015, then a short-lived drop to *c.* 2000 m^2 in late 2004/early 2005, roughly tracking the variability in MODIS FRP. The area of the south pit surrounding the lava lake increased from *c.* 19 000 m^2 in 2001 to *c.* 26 000 m^2 in late 2008, remaining fairly constant afterwards until the lava lake overflows of 2010 rendered the western pit rim impossible to identify. There does not appear to be any systematic bias between the areas digitized from ALI, ETM+ SLC-on and ETM+ SLC-off images, which all overlapped and follow the same trend. The high scatter about the trend for both area measurements is likely to be a function of the low resolution and noisy images used to digitize the features, leading to inaccuracies due to pixellation as well as the misidentification of features (e.g. confusion between the active lake, surrounding solidified crust and condensed gas emissions). However, despite the noisy time-series, the main trends could still be identified, highlighting the utility of moderate resolution datasets in measuring fine geomorphological changes when large numbers of images are available.

The variation in the depth of the bench below the eastern pit rim (bench depth) and the depth of the lava lake below the bench (lake depth) are shown in Figure 3g and h, respectively. Despite the scatter in the data, trends can be identified. The bench depth remained at roughly −80 m from 2000 to 2002, rose in the second half of 2002 to *c.* −50 m in early 2003 and remained roughly constant at *c.* −40 m from 2004 to November 2010, when it then rose again to *c.* −20 m, remaining at this height afterwards. There was significantly more scatter in the lake depth estimates, which were fewer in number as the ETM+ images were too coarse and noisy to reliably identify the lake shadow. The lake depth appears to have been *c.* −40 m in mid-2001, then to have been at bench level when the next available images were acquired in 2004.

There was significant scatter between 2005 and early 2008, with some implausibly low values with large error bars; however, the more accurate estimates appear to cluster around −30 m. The lake depth then rose to bench level again between mid-2008 and early 2011, with a few values of *c.* −30 m, and then fell to *c.* −20 m and remained at

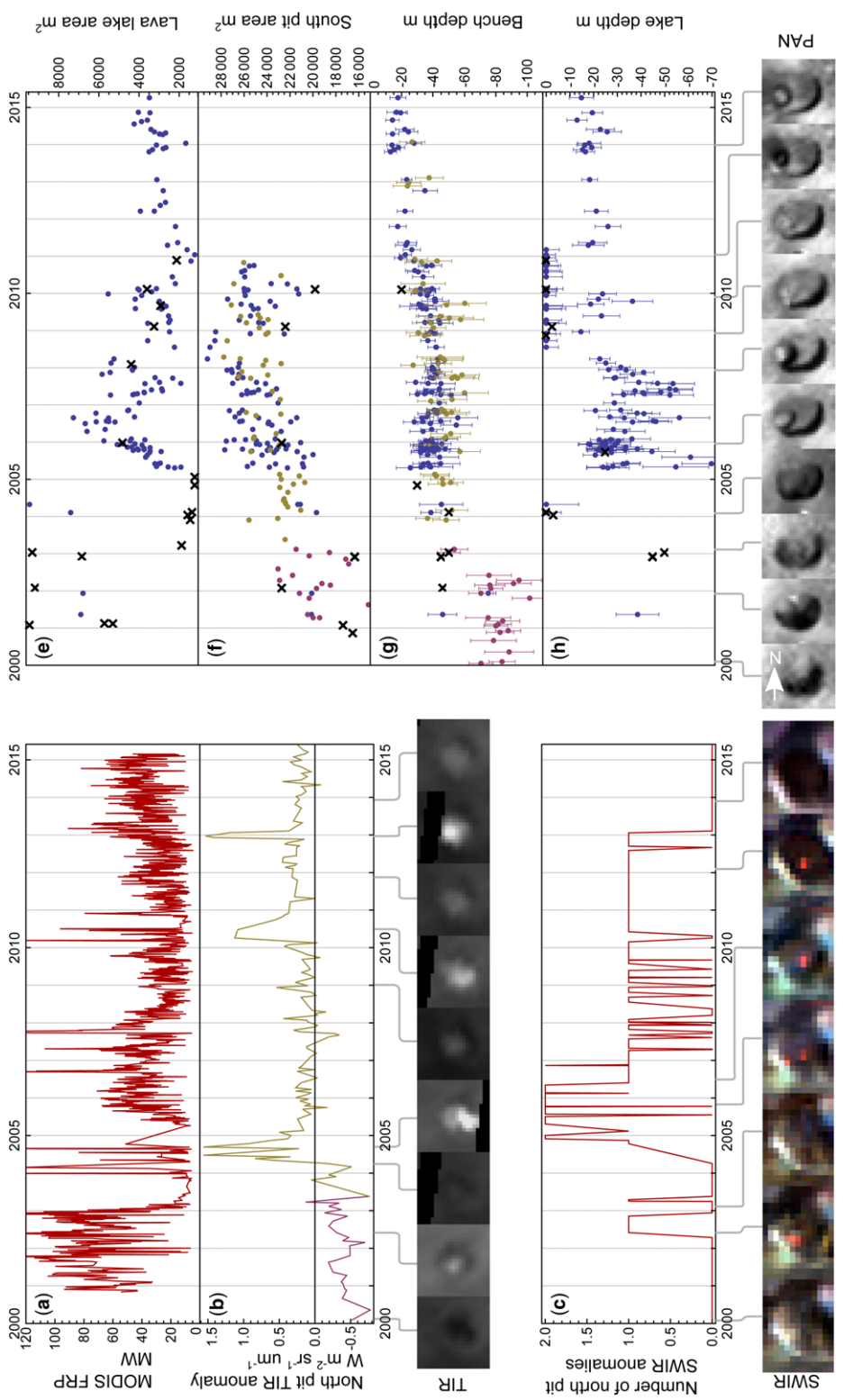

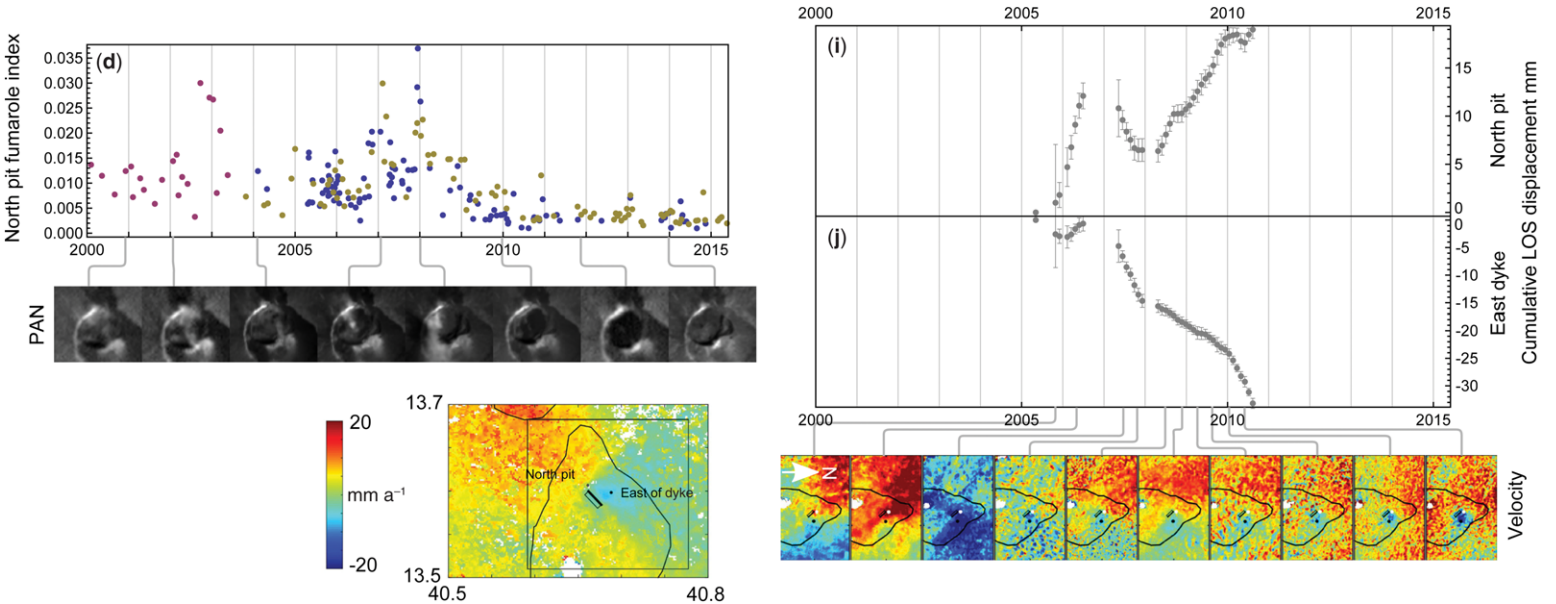

Fig. 3. Summary plot of all the time-series derived from Earth Observation data used in this study (except for the SEVIRI thermal anomaly). (**a**) MODIS-derived Fire Radiative Power (FRP) from the summit caldera region for nadir observations only. (**b**) North pit thermal infrared (TIR) anomaly time-series: Landsat 7 SLC-on data plotted in purple, SLC-off in yellow. Example TIR images from which the time-series is derived are shown as call-outs below. (**c**) Plot of the number of minor SWIR anomalies visible in the north pit in Landsat 7 and ALI images. Example SWIR images are shown as call-outs below. (**d**) North pit fumarole index time-series. ALI data plotted in blue, Landsat 7 SLC-on in purple, Landsat 7 SLC-off in yellow. Example panchromatic images showing patterns of condensed gas over the north pit are shown as call-outs below. (**e**) Lava lake area derived from ALI images. Black crosses are estimates from field observations reported in the literature and by the Smithsonian Global Volcanism Program. (**f**) South pit areas derived from ALI (blue), Landsat 7 SLC-on (purple) and Landsat 7 SLC-off (yellow), black crosses are field estimates. (**g**) Bench depth below eastern pit rim from ALI images (blue), Landsat 7 SLC-on (purple) and Landsat 7 SLC-off (yellow). Black crosses are field estimates. (**h**) Lava lake depth below bench from ALI images. Panchromatic images showing changing south pit morphology are shown as call-outs below. (**i**, **j**) cumulative line-of-sight (LOS) displacement of points centred in the north pit and over the 2004 dyke, respectively. Images of the spatial velocity distribution are shown as call-outs below and the mean velocity image is shown on the left. All velocity images have the same colour scale. Field observations were collated from the Smithsonian Global Volcanism Program (Global Volcanism Program 2001, 2003, 2004*a*, *b*, *c*, 2005*a*, *b*, *c*, 2006, 2008, 2009, 2010, 2011*a*), Volcano Discovery (2015) and previously published work (Field *et al.* 2012; Davies *et al.* 2011).

that level until 2015. The lake levels rose to bench level during periods where the bench was raised, as expected if it was constructed by successive overflows. Examples of the high-resolution panchromatic ALI and ETM+ images from which Figure 3e–h were derived are shown below the graphs. Note that as the lava lake became smaller between 2001 and 2015, it became less elliptical and more circular, as noted by Bouche *et al.* (2010).

Time-series of the cumulative LOS displacement between 2005 and 2010 for a point in the north pit and a point to the east of the 2004 dyke intrusion are shown in Figure 3i and j, respectively. Selected images of the incremental surface velocities are show below and the average velocity over the whole period is shown to the left. The time-series show a small, but persistent, deformation pattern consistent with a decrease in range (i.e. uplift) at the location east of the dyke intrusion and an increase in range (i.e. subsidence) at the north pit, since April 2008. The figures show that the surface velocity east of the dyke increased between mid-2009 and 2010, reaching a rate of range decrease of about 20 mm a^{-1} by August 2010. The time-series also show a fast range decrease at both sites between May and December 2007; however, we cannot exclude the fact that this may be a residual atmospheric artefact due to the high level of noise in the interferograms acquired in that period.

The deformation pattern observed at Erta 'Ale during 2008–10 is similar in extent and location to that caused by a dyke intrusion in 2004 (shown in Figs 1 & 4). The signal consists of range decrease extending mainly over the eastern side of the 2004 dyke and it is consistent with the continuous intrusion of magma into small dykes at this location. The best-fit solution for the dyke captured in the 2 January 2004 and 6 May 2005 interferograms (Fig. 4) consists of a 2.3 km long, 3.8 km wide, subvertical dyke with 0.26 m of uniform opening located at the southeastern edge of the summit caldera, roughly oriented along the regional trend of the Red Sea rift.

By inspection, a number of the time-series shown in Figure 3 appear to track each other – for example, the overall trend in MODIS FRP appears to be positively correlated with lake area and inversely correlated with the north pit TIR anomaly, whereas lake highstands appear to be associated with peaks in the north pit TIR and low background MODIS FRP with isolated peaks. However, it is difficult to plot the data against each other and verify this quantitatively because: (1) the observations were acquired irregularly at different temporal resolutions and at different times, necessitating some form of interpolation and smoothing to make them comparable; (2) the large measurement errors associated with some of the time-series make them very noisy, invalidating simple interpolation; and (3) the high degree of variability of some physical processes masks the overall trend.

To overcome these challenges and make the datasets comparable, we used first-order Tikhonov regularization to fit trend lines to the data to give one estimate of each variable per day, taking into account any available error estimates in the weighting matrix (Aster *et al.* 2011). The original data and fitted trend lines are shown in Figure 5a–e. To estimate the lava lake depth below the western pit, we added the lake depth below the bench and the bench depth below the rim to obtain the depth of the lake below the eastern pit rim. We then added 25 m to correct for the height difference between the east and west rims to obtain the lake height below the western pit rim. This made the time-series directly comparable with field observations, as shown in Figure 5f. In addition, due to the sparsity of estimates of the lake below the bench depth

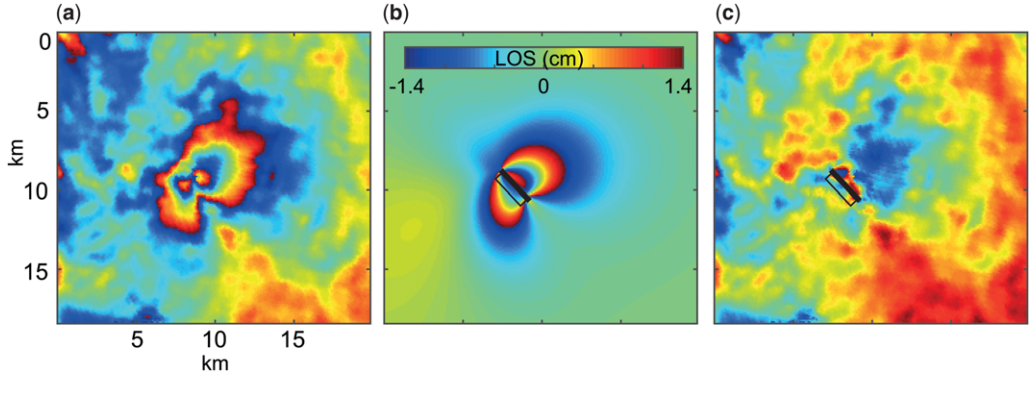

Fig. 4. (**a**) Interferogram spanning 2 January 2004 to 6 May 2005. (**b**) The best-fit model: a subvertical dyke 2.3 km long, 3.8 km wide with 0.26 m of uniform opening. (**c**) The residual.

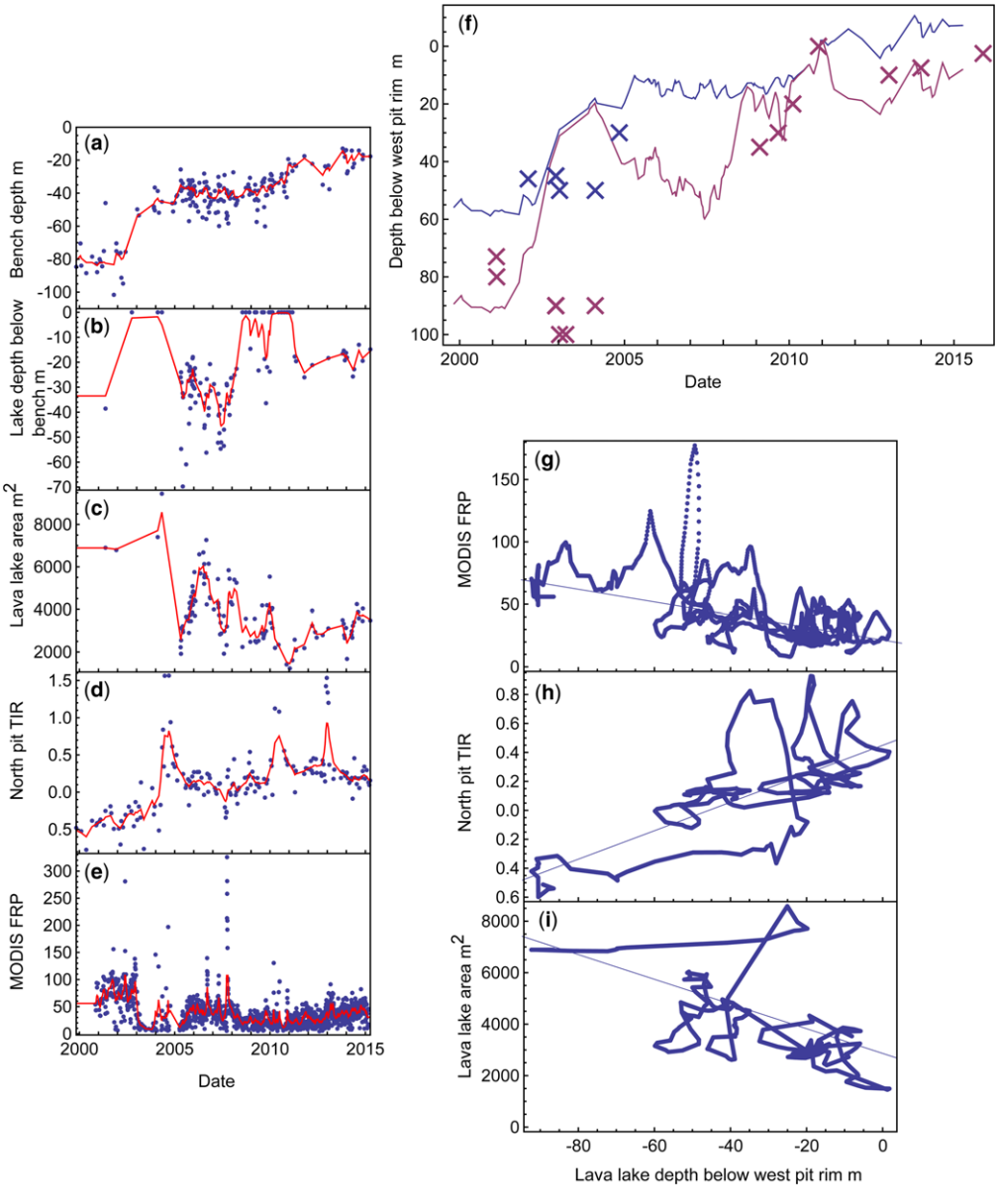

Fig. 5. Quantitative comparison of some of the time-series presented in Figure 3. (**a**–**e**) Original data (blue points) and best-fit trend line using first-order Thikonov regularization (red line) for bench depth below eastern pit rim, lake depth below bench, lake area, north pit thermal infrared (TIR) anomaly and MODIS Fire Radiative Power (FRP). (**f**) Lava lake depth (purple) and bench depth (blue) below the western pit rim, calculated by adding the regularized bench and lake depth time-series and adding a 25 m offset. Field observations are shown as purple and blue crosses. (**g**–**i**) Regularized time-series plotted against lava lake depth below west pit rim (blue points) with best-fit line shown in grey.

before 2005, we added a value of 0 at 1 October 2002, consistent with the lake needing to be at bench level to raise the height of the bench with overflows around this time.

The relationships between the variables are shown in Figure 5g–i. Lava lake depth below the west pit rim was found to be positively correlated with both MODIS FRP and lake area, with R^2 values

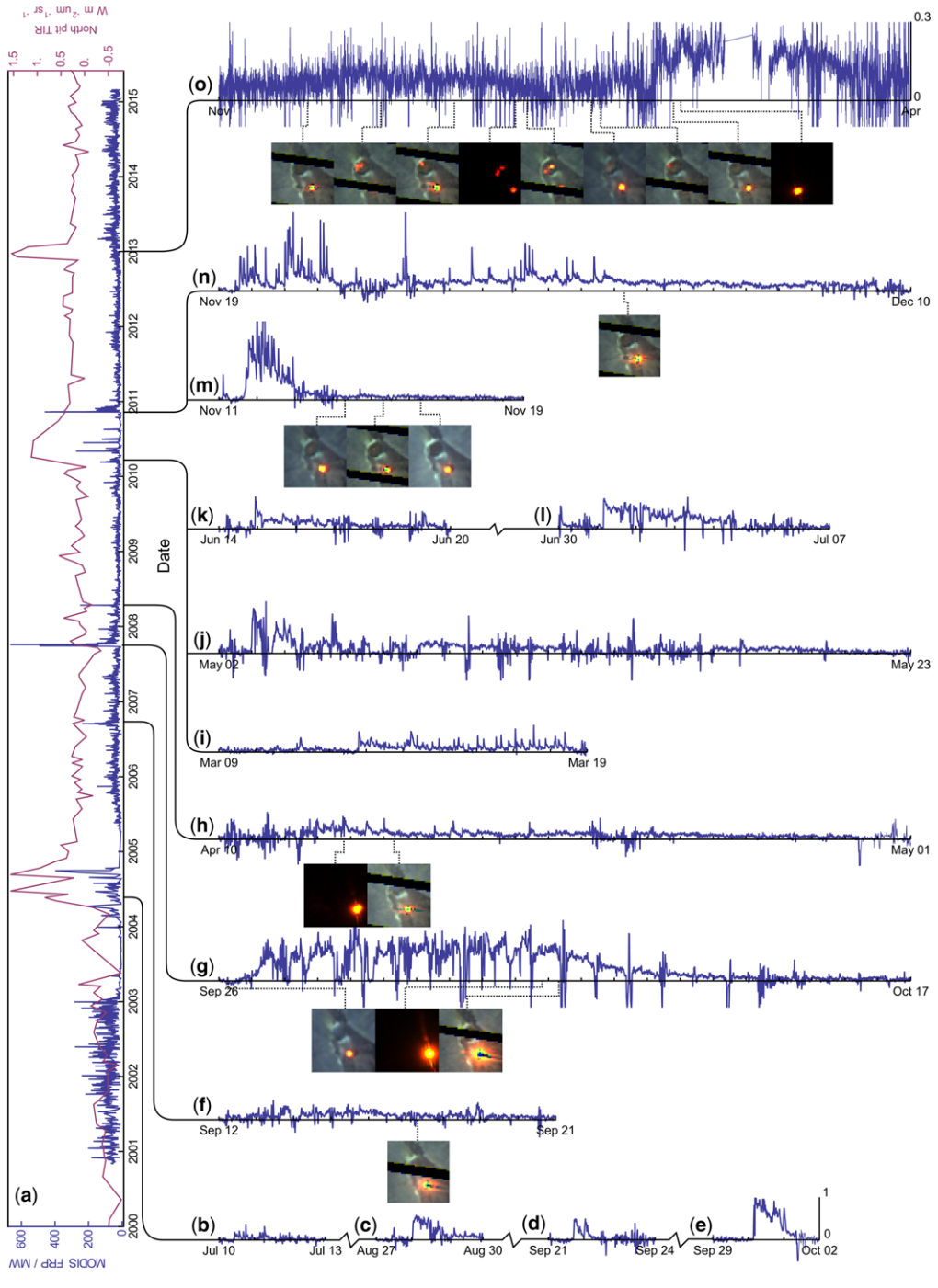

Fig. 6. Summary of the SEVIRI thermal anomaly time-series for the peaks in radiant output from the north and south pits. (**a**) Plot of MODIS Fire Radiative Power (FRP) for all view angles (blue line) and north pit TIR anomaly (purple line). The SEVIRI thermal anomalies associated with peaks in these variables are shown as call-outs to the right, with moderate resolution SWIR images acquired simultaneously shown below. Vertical scale is constant for plots (**b**–**n**); a smaller vertical scale is used for plot (**o**) to render the weaker signal visible; the horizontal scale is compressed for longer duration plots.

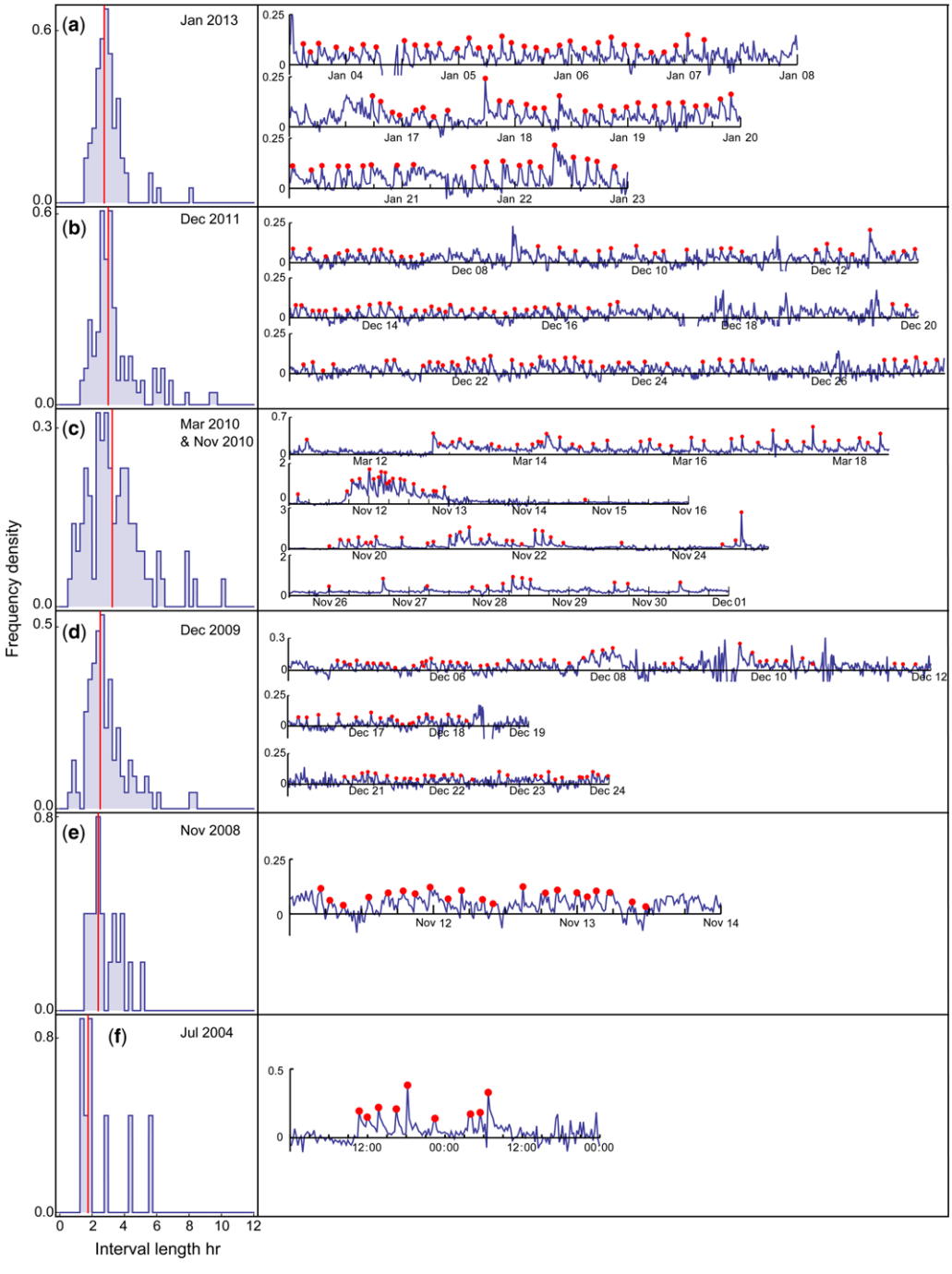

Fig. 7. Summary of the spike trains identified in the SEVIRI thermal anomaly time-series. For each period, the time-series is plotted on the right (lines) with selected spike peaks highlighted (dots). On the left, the inter-spike interval (ISI) histogram is shown with the median value highlighted. The median ISI values are: (**a**) 2.75 h, (**b**) 3 h, (**c**) 3.25 h, (**d**) 2.5 h, (**e**) 2.375 h and (**f**) 1.75 h.

of 0.39 and 0.55, respectively, and inversely correlated with the north pit TIR with an R^2 value of 0.41. Extrapolating the relationship for lake area and FRP gives a lake area of 0 at *c.* 60.0 m and an FRP of 0 at *c.* 42.5 m above the western pit rim, perhaps giving an upper limit to the height the lava lake can reach in the long term. Returning to Figure 3, there also appears to be a distinct change in early 2008, when (1) the fumarole index transitions from being high and variable to low and constant, (2) the gradual increase in the south pit area halts, (3) the second rise in lake level begins, (4) the north pit stops subsiding and starts uplifting and (5) the rate of subsidence at the east dyke decreases.

We used the MODIS FRP and north pit TIR anomalies to target acquisition of high-frequency SEVIRI images, allowing the investigation of peaks in radiant output in greater detail. We were able to identify whether each anomaly was sourced from the north pit or the lake by (1) examining Landsat-like high-resolution SWIR images acquired during the event to identify an instantaneous snapshot of activity, where available, and (2) by comparing the MODIS FRP and Landsat north pit anomaly time-series. This process is summarized in Figure 6. Some of the SEVIRI time-series are fairly noisy due to cloud cover, which manifests itself as an absence of any anomaly, or a succession of large, short-lived, negative and positive spikes during changeable cloud conditions (Barnie & Oppenheimer 2015*b*), but overall trends are visible and, where cloud is absent, short duration events of the order of an hour can be identified. The left-hand panel shows the MODIS FRP (all view angles) and north pit TIR anomaly time-series; the SEVIRI thermal anomaly time-series are plotted as callouts on the right-hand side. From bottom to top, the callouts show the detailed shape of the thermal anomalies associated with spikes in FRP and TIR from the start of SEVIRI data availability; July to October 2004, September 2006, September 2007, April 2008, March to November 2010 and November 2012 to April 2013.

The 2004 time-series is heavily affected by cloud, so here we show only four comparatively cloud-free snapshots in Figure 6b–e: one event in June that consists of a train of small spikes in radiance of a few hours duration each, and three events with a rapid onset/slow decay (rapid waxing, slow waning) shape. There was no simultaneous high-resolution image that allowed us to unambiguously identify the north pit or the lava lake as the source of these events; however, images acquired between these events (not shown here) showed SWIR thermal anomalies in the north pit. The picture is more complicated in the lake itself, with some images showing a greatly reduced lake anomaly and some showing an enlarged anomaly indicative of overflows. Given that the first spike in the north pit TIR anomaly covers this period, and between spikes the MODIS FRP is very low, we concluded that most of this activity took place in the north pit with greatly reduced activity in the south pit, despite occasional overflows.

The next major peak in MODIS FRP was identified in 2006 (Fig. 6f), which the SEVIRI time-series revealed as a broad, low amplitude rise and fall in radiance over about nine days. A single Landsat 7 SWIR image acquired in the middle of this time period placed the event in the lava lake. The 2007 MODIS FRP peak (Fig. 6g) had the highest power output of any peak during the study period and had the form of a slow increase in radiance in the SEVIRI anomaly over about a day, then around eight days of numerous small spikes in radiance superimposed on an elevated baseline (punctuated by periods of heavy cloud cover), followed by a smooth decay over about six days, without any superimposed spikes. One image acquired just before the event and two during the event showed that the lava lake was the source of the anomaly, which expanded and grew in intensity during this period.

The next FRP peak in 2008 (Fig. 6h) again showed a gradual onset, elevated radiance baseline with sparse superimposed spikes and a slow spikeless decay; the EO-1 and Landsat images again point to a source in the lava lake. The small FRP peak in March 2010 (Fig. 6i) consisted of a spike train superimposed on an elevated radiance baseline, although there were no high-resolution images to identify the source.

MODIS FRP peaks between May and August 2010 coincided with an increase in the north pit TIR anomaly and the SEVIRI thermal anomalies (Fig. 6j–l) returned to the pattern of sudden onset–slow decay previously seen in 2004 (although broken by heavy cloud cover). However, these anomalies were of longer duration on the order of a week or two, rather than a few days. Unfortunately, there were no high spatial resolution images to identify the source, although the images between the events (not shown here) did show significant SWIR anomalies in the north pit. The north pit TIR anomaly places these as probably the first events in the north pit since 2004. By November 2010, the north pit TIR anomaly had decayed, but significant FRP anomalies continued to occur and we returned to the pattern of a slowly waxing and waning baseline radiance with trains of superimposed spikes (Fig. 6m and n). Some of these spikes were observed by a field team, allowing us to identify this pattern of radiance unambiguously with lava lake overflows (Field *et al.* 2012). The SEVIRI dataset for November 2010 has been discussed in

detail in Field *et al.* (2012) and the analysis is not repeated here, except to re-iterate that the pattern of a slowly waxing and waning background anomaly with superimposed spike trains is consistent with the lava lake rising out of the view shadow of the sensor cast by the western pit rim into the field of view, generating spikes in radiance as the lake overflows on to the bench and caldera floor.

The final anomaly investigated occurred in late 2012 early 2013 and consisted of a substantial north pit TIR anomaly that lasted from the start of December 2012 to the end of January 2013 and a weak MODIS FRP anomaly that occurred between the end of January 2013 and the end of May 2013. Both these events show up in the SEVIRI anomaly as very weak, slowly varying, long-duration events (Fig. 6o). High-resolution SWIR images confirmed that the first event was associated with lava flows in the north pit, while the second appears to be sourced from the lava lake only.

A number of the SEVIRI anomalies identified in the previous section were associated with spike trains – a series of high-frequency spikes in radiance. We also looked for spike trains in periods without major thermal anomalies, but where relatively high MODIS FRP values and a high lava lake level indicated (1) a comparatively high level of thermal output and (2) that the SEVIRI instrument may have a direct view of the lake surface; we identified some extra spike trains in 2008, 2009 and 2011. We selected sequences of spikes that could be identified by eye above the instrument noise and cloud interference, grouped the sequences by year, manually selected the timing of each peak by the point of maximum radiance, and found the ISI histograms and median ISI value; these are summarized in Figure 7. The median ISI values lay between 1.75 hours in 2004 (Fig. 7f) and 3.25 hours in 2010 (Fig. 7c), with most values between 2.5 and 3.25.

A number of the lava lake events shown in detail in Figure 6 occurred close in time to regional magmatic and tectonic events. The timing of these regional events with respect to the MODIS FRP time-series is shown in Figure 8 and the events are described in Table 1. Specifically, the Erta 'Ale dyke (EAD) InSAR epoch spans the start of the period of isolated MODIS FRP spikes and rapid onset–slow waning SEVIRI anomalies in 2004, whereas the Dallol dyke occurred at the end of this period, the onset of the Manda Hararo rifting cycle occurred during the rejuvenation of the lava lake in late 2005 (as noted by Ayele *et al.* 2007*a*) and the MODIS FRP peaks in September 2006, September 2007 and November 2010 coincided with the fourth Manda Hararo dyke, the Jebel al Tair eruption and the Gulf of Aden seismic swarm, respectively. However, many of the regional events that occurred during the study period do not appear to be associated with substantial changes in lake behaviour, including the substantial Dalafilla fissure eruption just 26 km to the NW. There may be a small gap in the FRP time-series that could reflect sudden inactivation of the lake, perhaps due to a drop in magma supply induced by the nearby Dalafilla eruption, but this may also be a result of cloud.

To test whether there is a relationship between changes in lake activity and regional tectonic events, we split the FRP data into two categories, one containing all the FRP observations within a time window of the events (event FRP) and one containing the remaining observations (interval FRP), and compared their distributions. In this way, we could test whether the lava lake activity in the vicinity of events was similar to that between events, or whether it followed a different distribution. We log-transformed the FRP data to make it more Gaussian-like and therefore easier to display (Gaussian data is not, however, a requirement for the applied tests and the transformation did not affect the result). A histogram of all event and interval FRP data for a window of 20 days is shown in Figure 8. The distribution of event FRP is very different from that of interval FRP, being bimodal with the main mode shifted slightly to lower values and a smaller mode at high values, which is consistent with events occurring more often during periods of lower baseline power output and coinciding with localized high FRP peaks during this period.

The Kolmogorov–Smirnoff (KS) test gives a statistic of 1.9 with $p = 0.0019$, well below the typical significance level of 0.05, indicating that the two samples are unlikely to be drawn from the same distribution. However, the FRP time-series is autocorrelated in that high values tend to cluster together, which can invalidate the KS test (e.g. Durilleul & Legendre 1992). To check whether the autocorrelation had a large effect on the test, we calculated the KS statistic (the maximum difference between the empirical distribution functions for the two datasets) for 19 random events (equal to the number of observed events) and repeated this 1000 times to find the distribution of the KS statistic. The probability of obtaining a KS statistic as extreme or higher than that observed for real events was 0.34, so the autocorrelation appears to render the KS test more liberal in falsifying the null hypothesis. Varying the window size from 10 to 40 days gave probabilities of an as-extreme or more extreme KS statistic of 0.54 or greater, so we concluded that the null hypothesis (both samples drawn from the same distribution) could not be rejected at the 95% confidence level and that there was no statistically significant relationship between the short-term variation in power output and the occurrence of regional events.

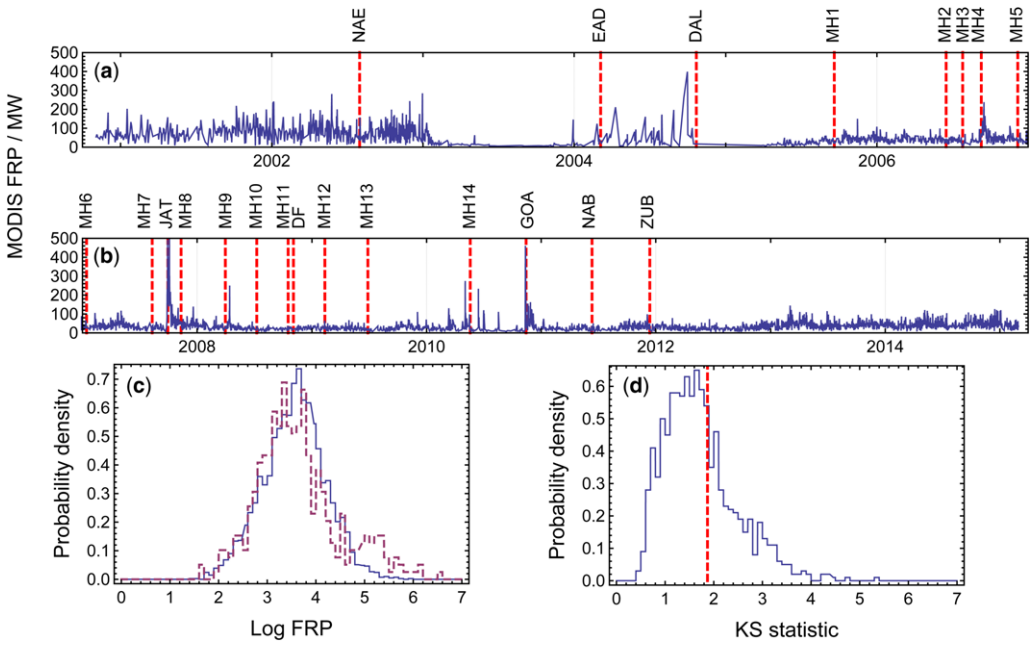

Fig. 8. (**a**, **b**) Timing of regional magmatic and tectonic events compared with MODIS Fire Radiative Power (FRP) (the regional events are described in Table 1). (**c**) Probability density histograms of FRP close in time to events (event FRP, dashed line) and between events (interval FRP, solid line). (**d**) Probability density histogram of the Kolmogorov–Smirnoff (KS) statistic for 19 random events, repeated 1000 times. The KS statistic for the real 19 events is shown as a vertical dashed line. DAL, Dallol dyke; DF, Dalaffilla; EA, Erta 'Ale; GOA, Gulf of Aden; JAT, Jebel al Tair; MH, Manda Hararo; NAB, Nabro; NAE, North Afar Earthquakes; ZUB, Zubair.

Discussion

Comparison with field observations

We compared our satellite observations with field observations reported in the literature and collated from scientists, tour groups and guides by the Smithsonian Global Volcanism Program and the website Volcano Discovery (Global Volcanism Program 2001, 2003, 2004*a*, *b*, *c*, 2005*a*, *b*, *c*, 2006, 2008, 2009, 2010, 2011*a*; Davies *et al.* 2011; Field *et al.* 2012; Volcano Discovery 2015). In general, we found good agreement, as shown in Figures 3 and 5. It should be noted, however, that although no error bar is plotted for the field observations, (1) we do not know how the observations were made and many appear to have been made 'by eye' and (2) many observations were rounded to the nearest 5 or 10 m, implying errors of a similar magnitude or more. Therefore where the satellite and field observations disagree, we do not necessarily dismiss the satellite observations out of hand.

The lake area digitized from EO-1 ALI images tracks the field observations well, as shown in Figure 3e, with a few high satellite-derived areas in 2004, perhaps as a result of images happening to catch extensive overflows from a persistently small lava lake, whereas field estimates of the south pit area fall within the point cloud of our estimates. Similarly, the depths of the bench below the pit rim and the lake below the bench lie within our point cloud of estimates, as do most of the estimates of lake depth below the western pit rim shown in Figure 5f. However, field estimates of the lake depth below the western pit rim appear to miss the rise in lake level height between 2002 and 2005. Given that our observations of the lake depth below the bench are sparse during this period, a rapid variation in lake height may resolve this apparent contradiction. The field estimates do not appear to capture the rise in the bench level in late 2002; however, there is a reference to more reasonable bench depths of 70 m prior to 2002, although a specific date is not mentioned.

The changes in activity reported in the north pit are also consistent with our observations, with fumarole emissions from the southern edge of the pit observed from November 2000 (Global Volcanism Program 2001) to January 2004 (Global Volcanism Program 2005*b*), while noisy fumaroles at the centre of a growing lava bulge at the centre of the north pit became evident in November 2004 (Global

Volcanism Program 2004*c*), consistent with emissions frequently appearing over the central small SWIR anomaly. The north pit is dynamic, with reports of collapses generating a series of terraces in 2008 along with a lava flow in November 2008, although this is not seen in the north pit TIR anomaly (Global Volcanism Program 2009). The presence of persistent small north pit anomalies between major events is consistent with repeated observations of small incandescent vents (e.g. November 2004; Global Volcanism Program 2004*c*) and the observation of an incandescent hornito in the pit centre in November 2010, which appeared extremely bright at night, with a recent large lava flow apparently sourced from the hornito covering the north pit floor, consistent with our placing a number of eruptive events in the north pit earlier in 2010 (Global Volcanism Program 2011*a*). We concluded that our satellite-derived observations were broadly consistent with the record of field observations.

Synthesis and interpretation

The diverse time-series we collated show the Erta 'Ale summit caldera region has exhibited a wide range of behaviour between 2000 and 2015, making generalizations difficult. However, we were able to make the following synthesis and interpretation.

The lava lake has risen by *c.* 80 m over the period 2000–15, with two distinct phases of rise and then fall during 2002–08 and 2008–11, with trough to peak amplitudes of *c.* 70 and *c.* 50 m, respectively.

The long-term pattern is that as the lake height increases, the lake area decreases, the lake power output decreases and the lake perimeter becomes less elliptical and more circular (the latter fact was also noted from field observations by Bouche *et al.* 2010). This is consistent with the lake adopting a more thermally efficient geometry by reducing the surface area through which heat is lost from the surface by radiation and convection and through the conduit walls by conduction to compensate for a greater heat loss during highstands. Both the relationships between lake height and MODIS FRP and lake area predict that the lake cannot be sustained more than 40–60 m above the present pit rim long term, given the current conditions.

If the lake height is predominantly determined by gas flux through the lava column, then the persistence of the Erta 'Ale lava lake may be dependent on the gas fluxes remaining low enough that the lake level remains within its allowable range; too low and the lake will be buried in the edifice, but too high and the lake level will rise and build an edifice until the area and power output reach zero, with hot material only being erupted during paroxysms as in a more conventional basaltic shield volcano. We speculate that persistent degassing through the north pit, caldera rim (which appears markedly discoloured on satellite images) or the flanks of the edifice may therefore be a requirement of a long-lived lava lake at Erta 'Ale. The lake height is positively correlated with the north pit thermal anomaly, consistent with the north pit and south pit being linked at depth, with lava flowing into the north pit as the lava head of the system rises, as noted by Le Guern *et al.* (1979) for the overflows of the early 1970s.

Superimposed on this first-order trend are a number of short-lived paroxysms in power output on a scale of days to weeks that can be traced back to either the north pit or lava lake. The lava lake paroxysms present in the SEVIRI thermal anomaly as a slowly waxing and waning pattern, usually with superimposed spike trains. Events of this type occurred in July 2004, September 2006 and 2007, April 2008, November 2010 and perhaps March 2013. Field observations in 2010 by Field *et al.* (2012) indicate that the slow waxing and waning reflects the slow rise and fall of the lake surface into and out of the SEVIRI sensor field of view, whereas the spikes during the waxing phase are overflows onto the bench or the caldera as the lake level rises. Their absence during the waning phase reflects the inability of the lake surface to overflow while confined in the conduit.

These overflows are responsible for raising the level of the bench, although this only occurred substantially in 2002 and November 2010. The latter period was associated with two prominent slow waxing–waning events, whereas the former does not appear to be associated with any unusually high power output, although it is plausible the signal was 'lost' in the higher and more variable MODIS FRP output during this period. Sadly, the SEVIRI archive does not extend far enough back in time to investigate this earlier 'stealth' rise in lake level in more detail. The lava lake paroxysms exhibit increases in power output with rises in lake level and overflows, contradicting the overall pattern and indicating that the system can depart from the baseline trade-off between height and power/area, at least in the short term, perhaps due to simultaneous increases in gas and heat flux.

The lava lake highstands of 2004 and 2010 were both associated with significant eruptions in the north pit. These stand in contrast with the lava lake paroxysms in that they exhibit a rapid waxing and slow waning pattern consistent with the Wadge (1981) model for the failure of a pressurized magma chamber driving variations in the effusion rates, as seen in satellite data during fissure eruptions on Etna and Krafla (Harris *et al.* 2000). Unfortunately, we were unable to find any eyewitness accounts of these events because they occurred in

the hotter months when visits were infrequent and there were no simultaneous Landsat-like satellite image acquisitions. However, the residual heat detected in the north pit TIR time-series indicated these were most probably eruptions in the north pit. The 2010 events were significantly longer than the 2004 events, perhaps indicating easier magma pathways to the surface due to the repeated intrusion of previously emplaced hot material, or perhaps simply an increase in the magma supply.

The final eruption in the north pit between December 2012 and January 2013 was a slow waxing and waning event around two months in duration, more typical of slowly varying open vent activity at the lava lake than the previous sudden eruptions in the north pit. We interpret this as a continuation of the tendency towards longer duration events, with an open vent to the surface now established, which allowed lava to slowly leak out, without the requirement for the build-up of pressure to force new intrusions. This may represent the closest the northern lava lake has come to reactivating since the 1980s. However, the small hornitos visible in the SWIR between major eruptive phases since the first rise in lake level in 2002 disappeared after the 2012–13 event, which may indicate that this pathway has been shut off and/or the lava supply to the north pit has reduced.

There appears to have been a summit caldera-wide discontinuity in activity in early 2008, which affected the long-term trends in a number of variables. The north pit fumarole index decreased, indicating a reduction in condensed gases over the pit; the area of the south pit stopped expanding; the north pit stopped uplifting and started to subside; and the uplift of the east dyke slowed down. In addition, there were reports of a 'massive collapse' in the north pit during 2008 (Global Volcanism Program 2009). All of this occurred as the second rise in lake level height began and so may have been a response to the injection of new gas-rich magma into the system. However, there was no similar change in these indicators during the first rise in lake level in late 2002.

The spikes in the spike trains visible in July 2004, March 2010 and November 2010 all have fairly prominent peaks and occurred at times when the lake was at bench level. Combined with field observations of the overflows in November 2010 (Field *et al.* 2012), these can be confidently identified as overflows as a result of vertical fluctuations in the height of the lava lake. The spike trains in December 2011 and January 2013 occurred when the lake was elevated (*c.* −20 m) and was therefore in the sensor field of view, but still below the bench and/or caldera and unable to overflow. These spike trains also lacked the exaggerated peaks of the overflows. We therefore interpreted these as recording fluctuations in radiant output during the resurfacing cycle, rather than as individual overflows. Despite occurring during a highstand at bench level, the low amplitude of the December 2009 and November 2008 spike trains may also indicate they were a record of the resurfacing cycle. The fact that all of the spikes trains from 2008 onwards had similar median ISIs indicates that: (1) the vertical oscillations that gave rise to overflows and the resurfacing cycle that gave rise to fluctuations in radiant output due to variations in surface temperature had similar periods and may be two aspects of the same phenomenon; and (2) short timescale cyclicity in the activity of the lava lake is remarkably constant throughout a changeable period at Erta 'Ale and the processes driving it are probably independent of the height, area and power output of the lake.

There does not appear to be a statistically significant relationship between power output from the summit region and the timing of regional events. There were some coincidences: between EAD and the Dallol dyke and the onset and cessation of north pit eruptions in 2004, respectively; Manda Hararo rifting cycle 1 with the slow rejuvenation of the lava lake in 2005; and the fourth Manda Hararo dyke, Jebel al Tair and Gulf of Aden with lava lake paroxysms in 2006, 2007 and 2010. Despite this, many regional events do not correlate with changes in lake activity and there is a significant chance of finding such coincidences with regional events randomly located in time. However, there may still be a relationship over longer timescales, as the change in behaviour at Erta 'Ale stating with the rise in lake level in 2002 (1) pre-empts an apparent regional upsurge in magmatic–tectonic events over the following decade and (2) appears to be the first major change at the lava lake since the overflows of the early 1970s, which themselves preceded the Asal Ghoubbett rifting event in November 1978 (Allard *et al.* 1979). This may indicate that Erta 'Ale responds to region-wide developments on a timescale of years to decades and anticipates them, perhaps due to the open vent nature of the volcano rendering subtle perturbations at depth visible more rapidly at the surface than other magmatic systems. Lava lakes could thus serve as a 'canary in the mine' for increases in regional activity.

Testing this longer-term hypothesis requires the integration of a much wider range of EO data, along with a comprehensive survey of activity on a decadal scale, which is challenging in a sparsely monitored region and is beyond the scope of this paper. We also cannot discount the potential for more spatially localized relationships. If we restrict the analysis to events on the Erta 'Ale range, there appear to be more coincidences, with the EAD being associated with the first north pit eruptions

and the Dallol dyke in the north with their cessation. However, the large Dalafilla fissure eruption does not appear to have had a major impact. In summary, we believe we can rule out a relationship between regional events and variations in power output on a timescale of days to weeks. In addition, the evidence for synchronicity in the timings of events at neighbouring volcanic centres in the Erta ‘Ale range is weak, although the Erta ‘Ale lava lake may track variations in regional activity on a decadal scale. However, this requires much longer datasets to establish, perhaps supplemented by comparison with similar open vent systems elsewhere.

The EAD occurs during the first lava lake highstand and the InSAR epoch spans the onset of the period of eruptions in the north pit, thus both may be a consequence of an increase in the head of lava in the system. However, continued deformation in the intruded region following a similar pattern over the following five years indicates the continuous intrusion of magma and may indicate that the dyke has a role in supplying magma to the system. This may imply that repeated dyke intrusions play a key part in maintaining persistent lava lakes. It is also notable that the lava lake and north pit paroxysms only occurred after the EAD, which may imply that these short duration events that deviate from the long-term height–power/area trend are caused by influxes of over-pressurized hot/gas-rich fresh magma during these repeated intrusions.

Conclusions

We draw the following conclusions from our analysis:

(1) Contemporary freely available Earth Observation datasets can be combined to provide detailed time-series of measurements and indices of geometric and radiometric changes at a range of temporal and spatial scales of activity in remote regions and can be adequately ground-truthed using sporadic eyewitness reports. In particular, slow changes in small-scale geomorphological features can be identified in comparatively coarse resolution satellite images despite large errors if large numbers of estimates are made. High time resolution/low spatial resolution geostationary weather satellites can be used to resolve surprisingly small events down to individual lava lake resurfacing cycles on a timescale of hours. Where a parameter of interest cannot be measured directly (e.g. gas fluxes), proxies can be found that, although imperfect, do reveal trends if a sufficient density and duration of observations can be achieved.

(2) The Erta ‘Ale lava lake has undergone two cycles of lava lake rise and fall between 2000 and 2015, with a net gain in height of *c.* 80 m. As the lake level rises, the geometry of the lava lake appears to change in response to increased heat loss, becoming smaller and more circular with reduced radiant power output, imposing a maximum height that the lake can reach of between *c.* 40 and *c.* 60 m above the south pit rim, which may reflect a fundamental constraint on the persistence of lava lakes. Superimposed on this trend are short-term paroxysms at the lava lake and in the north pit, which manifest as rising lava lake levels and overflows in the lake and fissure-type eruptions in the north pit. The lava lake paroxysms depart from the height–area/power trade-off and start after the EAD intrusion in early 2004, perhaps implying that these paroxysms are related to the repeated re-intrusion of this dyke supplying over-pressurized hot gassy magma to the summit magma chamber system. This also implicates dykes in an important role in supplying magma to the feeder system and maintaining persistent lava lakes. The lava lake overflows and the resurfacing cycle have similar periods (*c.* 3 h), implying that they are two aspects of the same process, which varies little despite fluctuations in lake geometry and power output. Between 2000 and 2015, repeated eruptions in the north pit evolved from fissure eruptions to longer duration fluctuations similar to those seen at the lava lake, which may indicate that the northern lava lake came close to reactivating in 2013.

(3) Eruptions in the north pit and paroxysms in the lava lake on a scale of days to weeks do not appear to be correlated with regional magmatic and tectonic events; however, broader multiyear fluctuations in the height of the lava lake may be associated with the regional increases in activity. Our future work will address long-term fluctuations in lava lake activity on a multi-decadal timescale.

We thank S. Calvari and an anonymous reviewer for their helpful comments. This research was undertaken as part of the NERC consortium project ‘How does the Earth’s crust grow at divergent plate boundaries? A unique opportunity in Afar, Ethiopia’ (grant number NE/E005535/1). CO is additionally supported by the National Centre for Earth Observation (Dynamic Earth and Geohazards theme). The MCD14ML Global Monthly Fire Location Product dataset was produced by the University of Maryland and provided by NASA FIRMS operated by NASA/GSFC/ESDIS with funding provided by NASA/HQ.

Available online: https://earthdata.nasa.gov/active-fire-data#tab-content-6. Landsat 7 Enhanced Thematic

Mapper + and Earth Observing 1 Advanced Land Imager images courtesy of the US Geological Survey. Spinning Enhanced Visible and InfraRed Imager data courtesy of EUMETSAT.

References

AHMED, A., DOUBRE, C. *ET AL.* 2016. Seafloor spreading event in western Gulf of Aden during the November 2010–March 2011 period captured by regional seismic networks: Evidence for diking events and interactions with a nascent transform zone. *Geophysical Journal International*, first published online February 22, 2016, http://doi.org/10.1093/gji/ggw068

ALLARD, P., TAZIEFF, H. & DAJLEVIC, D. 1979. Observations of seafloor spreading in Afar during the November 1978 fissure eruption. *Nature*, **279**, 30–33, http://doi.org/10.1038/279030a0

AMELUNG, F., OPPENHEIMER, C., SEGALL, P. & ZEBKER, H. 2000. Ground deformation near Gada 'Ale Volcano, Afar, observed by radar interferometry. *Geophysical Research Letters*, **27**, 3093–3096.

AMINOU, D.M.A. 2002. MSG's SEVIRI instrument. *European Space Agency Bulletin*, **111**, 15–17.

AMINOU, D.M.A., JACQUET, B. & PASTERNAK, F. 1997. Characteristics of the Meteosat second generation (MSG) radiometer/imager: SEVIRI. *In*: FUJISADA, H. (ed.) *Sensors, Systems, and Next-Generation Satellites*. SPIE Proceedings, **3221**, 19–31.

ASTER, R.C., BORCHERS, B. & THURBER, C.H. 2011. *Parameter Estimation and Inverse Problems*. 2nd edn. Elsevier.

AYELE, A., JACQUES, E. *ET AL.* 2007*a*. The volcano-seismic crisis in Afar, Ethiopia, starting September 2005. *Earth and Planetary Science Letters*, **255**, 177–187.

AYELE, A., STUART, G., BASTOW, I. & KEIR, D. 2007*b*. The August 2002 earthquake sequence in north Afar: insights into the neotectonics of the Danakil microplate. *Journal of African Earth Sciences*, **48**, 70–79, http://doi.org/10.1016/j.jafrearsci.2006.06.011

AYELE, A., KEIR, D. *ET AL.* 2009. September 2005 mega-dike emplacement in the Manda–Harraro nascent oceanic rift (Afar depression). *Geophysical Research Letters*, **36**, http://doi.org/10.1029/2009GL039605

BALL, M. & PINKERTON, H. 2006. Factors affecting the accuracy of thermal imaging cameras in volcanology. *Journal of Geophysical Research*, **111**, B11203.

BARBERI, F. & VARET, J. 1970. The Erta Ale volcanic range (Danakil Depression, northern Afar, Ethiopia). *Bulletin Volcanologique*, **34**, 848–917.

BARBERI, F., BORSI, S., FERRARA, G., MARINELL, G. & VARETS, J. 1970. Relations between tectonics and magmatology in northern Danakil Depression (Ethiopia). *Philosophical Transactions of the Royal Society of London Series A*, **267**, 293–311.

BARBERI, F., TAZIEFF, H. & VARET, J. 1972. Volcanism in Afar Depression – its tectonic and magmatic significance. *Tectonophysics*, **15**, 19–29.

BARBERI, F., CHEMINEE, J.L. & VARET, J. 1973. Long-lived lava lakes of Erta Ale volcano. *Revue de géographie physique et de géologie dynamique*, **15**, 347–351.

BARNIE, T.D. & OPPENHEIMER, C. 2015*a*. Inverting multispectral thermal time-series images of volcanic eruptions for lava emplacement models. *In*: HARRIS, A.J.L., DE GROEVE, T., GAREL, F. & CARN, S.A. (eds) *Detecting, Modelling and Responding to Effusive Eruptions*. Geological Society, London, Special Publications, **426**. First published online July 8, 2015, http://doi.org/10.1144/SP426.13

BARNIE, T.D. & OPPENHEIMER, C. 2015*b*. Extracting High Temperature Event radiance from satellite images and correcting for saturation using Independent Component Analysis. *Remote Sensing of Environment*, **158**, 56–68.

BARNIE, T.D., KEIR, D. *ET AL.* 2015. A multidisciplinary study of the final episode of the Manda Hararo dyke sequence, Ethiopia, and implications for trends in volcanism during the rifting cycle. *In*: WRIGHT, T.J., AYELE, A., FERGUSON, D.J., KIDANE, T. & VYE-BROWN, C. (eds) *Magmatic Rifting and Active Volcanism*. Geological Society, London, Special Publications, **420**. First published online May 12, 2015, http://doi.org/10.1144/SP420.6

BELACHEW, M., EBINGER, C., COTÉ, D., KEIR, D., ROWLAND, J.V., HAMMOND, J.O.S. & AYELE, A. 2011. Comparison of dike intrusions in an incipient seafloor-spreading segment in Afar, Ethiopia: seismicity perspectives. *Journal of Geophysical Research*, **116**, B06405, http://doi.org/10.1029/2010jb007908

BOUCHE, E., VERGNIOLLE, S. *ET AL.* 2010. The role of large bubbles detected from acoustic measurements on the dynamics of Erta 'Ale lava lake (Ethiopia). *Earth and Planetary Science Letters*, **295**, 37–48, http://doi.org/10.1016/j.epsl.2010.03.020

BURGI, P.-Y., CAILLET, M. & HAEFELI, S. 2002. Field temperature measurements at Erta 'Ale Lava Lake, Ethiopia. *Bulletin of Volcanology*, **64**, 472–485, http://doi.org/10.1007/s00445-002-0224-3

CERVELLI, P., MURRAY, H., SEGALL, P., AOKI, Y. & KATO, T. 2001. Estimating source parameters from deformation data, with an application to the March 1997 earthquake swarm off the Izu Peninsula, Japan. *Journal of Geophysical Research*, **106**, 11217–11237, http://doi.org/10.1029/2000JB900399

CHANDER, G., MARKHAM, B.L. & HELDER, D.L. 2009. Summary of current radiometric calibration coefficients for Landsat MSS, TM, ETM+, and EO-1 ALI sensors. *Remote Sensing of Environment*, **113**, 893–903, http://doi.org/10.1016/j.rse.2009.01.007

DARWIN, C. 1840. XLII. – On the Connexion of certain volcanic phenomena in South America; and on the formation of mountain chains and volcanos, as the effect of the same power by which continents are elevated. *Transactions of the Geological Society of London, Series 2*, **5**, 601–631, http://doi.org/10.1144/transgslb.5.3.601

DAVIES, A.G. 1996. Io's volcanism: thermo-physical models of silicate lava compared with observations of thermal emission. *Icarus*, **124**, 45–61, http://doi.org/10.1006/icar.1996.0189

DAVIES, A.G., CHIEN, S. *ET AL.* 2006. Monitoring active volcanism with the Autonomous Sciencecraft Experiment on EO-1. *Remote Sensing of Environment*, **101**, 427–446, http://doi.org/10.1016/j.rse.2005.08.007

DAVIES, D.K., ILAVAJHALA, S., WONG, M.M. & JUSTICE, C.O. 2009. Fire Information for Resource Management

System: archiving and distributing MODIS active fire data. *IEEE Transactions on Geoscience and Remote Sensing*, **47**, 72–79, http://doi.org/10.1109/tgrs.2008.2002076

Davies, A.G., Keszthelyi, L. & Harris, A.J.L. 2010. The thermal signature of volcanic eruptions on Io and Earth. *Journal of Volcanology and Geothermal Research*, **194**, 75–99, http://doi.org/10.1016/j.jvolgeores.2010.04.009

Davies, A.G., Keszthelyi, L. & McEwen, A.S. 2011. Estimating eruption temperature from thermal emission spectra of lava fountain activity in the Erta 'Ale (Ethiopia) volcano lava lake: implications for observing Io's volcanoes. *Geophysical Research Letters*, **38**, L21308, http://doi.org/10.1029/2011GL0 49418

Donegan, S.J. & Flynn, L.P. 2004. Comparison of the response of the Landsat 7 Enhanced Thematic Mapper Plus and the Earth Observing-1 Advanced Land Imager over active lava flows. *Journal of Volcanology and Geothermal Research*, **135**, 105–126, http://doi.org/10.1016/j.jvolgeores.2003.12.010

Durilleul, P. & Legendre, P. 1992. Lack of robustness in two tests of normality against autocorrelation in sample data. *Journal of Statistical Computation and Simulation*, **42**, 79–91, http://doi.org/10.1080/00949659208811412

Ebinger, C., Ayele, A. *et al.* 2010. Length and timescales of rift faulting and magma intrusion: the Afar rifting cycle from 2005 to present. *Annual Review of Earth and Planetary Sciences*, **38**, 439–466.

Eggert, S. & Walter, T.R. 2009. Volcanic activity before and after large tectonic earthquakes: observations and statistical significance. *Tectonophysics*, **471**, 14–26, http://doi.org/10.1016/j.tecto.2008.10.003

Ferguson, D.J., Barnie, T.D. *et al.* 2010. Recent rift-related volcanism in Afar, Ethiopia. *Earth and Planetary Science Letters*, **292**, 409–418, http://doi.org/10.1016/j.epsl.2010.02.010

Field, L., Barnie, T., Blundy, J., Brooker, R.A., Keir, D., Lewi, E. & Saunders, K. 2012. Integrated field, satellite and petrological observations of the November 2010 eruption of Erta 'Ale. *Bulletin of Volcanology*, **74**, 2251–2271, http://doi.org/10.1007/s00445-012-0660-7

Flynn, L.P., Harris, A.J.L. & Wright, R. 2001. Improved identification of volcanic features using Landsat 7 ETM+. *Remote Sensing of Environment*, **78**, 189–193, http://doi.org/10.1016/S0034-4257 (01)00258-9

Ganci, G., Vicari, A., Fortuna, L. & Del Negro, C. 2011. The HOTSAT volcano monitoring system based on combined use of SEVIRI and MODIS multispectral data. *Annals of Geophysics*, **54**, http://doi.org/10.4401/ag-5338

Gerlach, T.M. 1980. Investigation of volcanic gas analyses and magma outgassing from Erta' Ale lava lake, Afar, Ethiopia. *Journal of Volcanology and Geothermal Research*, **7**, 415–441, http://doi.org/10.1016/0377-0273(80)90041-4

Giglio, L. 2013. MODIS Collection 5 Active Fire Product User's Guide Version 2.5, http://modis-fire.umd.edu/files/MODIS_Fire_Users_Guide_2.5.pdf

Giglio, L., Descloitres, J., Justice, C.O. & Kaufman, Y.J. 2003. An enhanced contextual fire detection algorithm for MODIS. *Remote Sensing of Environment*, **87**, 273–282, http://doi.org/10.1016/s0034-4257(03)00184-6

Global Volcanism Program 1992. Report on Erta Ale (Ethiopia). *In*: McClelland, L. (ed.) *Bulletin of the Global Volcanism Network, 17:11*. Smithsonian Institution, Washington DC.

Global Volcanism Program 2001. Report on Erta Ale (Ethiopia). *In*: Wunderman, R. (ed.) *Bulletin of the Global Volcanism Network, 26:12*. Smithsonian Institution, Washington DC, http://doi.org/10.5479/si.GVP.BGVN200112-221080

Global Volcanism Program 2003. Report on Erta Ale (Ethiopia). *In*: Venzke, E. (ed.) *Bulletin of the Global Volcanism Network, 28:4*. Smithsonian Institution, Washington DC, http://doi.org/10.5479/si.GVP.BGVN200304-221080

Global Volcanism Program 2004*a*. Report on Erta Ale (Ethiopia). *In*: Venzke, E. (ed.) *Bulletin of the Global Volcanism Network, 29:2*. Smithsonian Institution, Washington DC, http://doi.org/10.5479/si.GVP.BGVN200402-221080

Global Volcanism Program 2004*b*. Report on Erta Ale (Ethiopia). *In*: Wunderman, R. (ed.) *Bulletin of the Global Volcanism Network, 29:8*. Smithsonian Institution, Washington DC, http://doi.org/10.5479/si.GVP.BGVN200408-221080

Global Volcanism Program 2004*c*. Report on Erta Ale (Ethiopia). *In*: Wunderman, R. (ed.) *Bulletin of the Global Volcanism Network, 29:11*. Smithsonian Institution, Washington DC, http://doi.org/10.5479/si.GVP.BGVN200411-221080

Global Volcanism Program 2005*a*. Report on Erta Ale (Ethiopia). *In*: Wunderman, R. (ed.) *Bulletin of the Global Volcanism Network, 30:1*. Smithsonian Institution, Washington DC.

Global Volcanism Program 2005*b*. Report on Erta Ale (Ethiopia). *In*: Venzke, E. (ed.) *Bulletin of the Global Volcanism Network, 30:7*. Smithsonian Institution, Washington DC, http://doi.org/10.5479/si.GVP.BGVN200507-221080

Global Volcanism Program 2005*c*. Report on Erta Ale (Ethiopia). *In*: Wunderman, R. (ed.) *Bulletin of the Global Volcanism Network, 30:09*. Smithsonian Institution, Washington DC, http://doi.org/10.5479/si.GVP.BGVN200509-221080

Global Volcanism Program 2006. Report on Erta Ale (Ethiopia). *In*: Wunderman, R. (ed.) *Bulletin of the Global Volcanism Network, 31:3*. Smithsonian Institution, Washington DC, http://doi.org/10.5479/si.GVP.BGVN200603-221080

Global Volcanism Program 2008. Report on Erta Ale (Ethiopia). *In*: Wunderman, R. (ed.) *Bulletin of the Global Volcanism Network, 33:6*. Smithsonian Institution, Washington DC, http://doi.org/10.5479/si.GVP.BGVN200806-221080

Global Volcanism Program 2009. Report on Erta Ale (Ethiopia). *In*: Wunderman, R. (ed.) *Bulletin of the Global Volcanism Network, 34:7*. Smithsonian Institution, Washington DC.

Global Volcanism Program 2010. Report on Erta Ale (Ethiopia). *In*: Wunderman, R. (ed.) *Bulletin of the Global Volcanism Network, 35:1*. Smithsonian Institution, Washington DC, http://doi.org/10.5479/si.GVP.BGVN201001-221080

Global Volcanism Program 2011*a*. Report on Erta Ale (Ethiopia). *In*: Wunderman, R. (ed.) *Bulletin of the Global Volcanism Network, 36:6*. Smithsonian Institution, Washington DC, http://doi.org/10.5479/si.GVP.BGVN201106-221080

Global Volcanism Program 2011*b*. Report on Zubair Group (Yemen). *In*: Wunderman, R. (ed.) *Bulletin of the Global Volcanism Network, 36:11*. Smithsonian Institution, Washington DC.

Goitom, B., Oppenheimer, C. *et al.* 2015. First recorded eruption of Nabro volcano, Eritrea, 2011. *Bulletin of Volcanology*, **77**, http://doi.org/10.1007/s00445-015-0966-3

Goward, S.N., Masek, J.G., Williams, D.L., Irons, J.R. & Thompson, R.J. 2001. The Landsat 7 mission: terrestrial research and applications for the 21st century. *Remote Sensing of Environment*, **78**, 3–12, http://doi.org/10.1016/S0034-4257(01)00262-0

Grandin, R., Socquet, A. *et al.* 2009. September 2005 Manda Hararo-Dabbahu rifting event, Afar (Ethiopia): constraints provided by geodetic data. *Journal of Geophysical Research*, **114**, B08404, http://doi.org/10.1029/2008jb005843

Hamling, I.J., Ayele, A. *et al.* 2009. Geodetic observations of the ongoing Dabbahu rifting episode: new dyke intrusions in 2006 and 2007. *Geophysical Journal International*, **178**, 989–1003, http://doi.org/10.1111/j.1365-246X.2009.04163.x

Hamlyn, J.E., Keir, D. *et al.* 2014. Seismicity and subsidence following the 2011 Nabro eruption, Eritrea: insights into the plumbing system of an off-rift volcano. *Journal of Geophysical Research*, **119**, 8267–8282, http://doi.org/10.1002/2014jb011395

Harris, A.J.L. 2008. Modeling lava lake heat loss, rheology, and convection. *Geophysical Research Letters*, **35**, L07303, http://doi.org/10.1029/2008gl033190

Harris, A.J.L., Flynn, L.P., Rothery, D.A., Oppenheimer, C. & Sherman, S.B. 1999. Mass flux measurements at active lava lakes: implications for magma recycling. *Journal of Geophysical Research*, **104**, 7117–7136, http://doi.org/10.1029/98jb02731

Harris, A.J.L., Murray, J.B. *et al.* 2000. Effusion rate trends at Etna and Krafla and their implications for eruptive mechanisms. *Journal of Volcanology and Geothermal Research*, **102**, 237–269, http://doi.org/10.1016/S0377-0273(00)00190-6

Harris, A.J.L., Carniel, R. & Jones, J. 2005. Identification of variable convective regimes at Erta 'Ale Lava Lake. *Journal of Volcanology and Geothermal Research*, **142**, 207–223, http://doi.org/10.1016/j.jvolgeores.2004.11.011

Hayward, N.J. & Ebinger, C.J. 1996. Variations in the along-axis segmentation of the Afar Rift system. *Tectonics*, **15**, 244–257.

Hill, D.P., Reasenberg, P.A. *et al.* 1993. Seismicity remotely triggered by the magnitude 7.3 Landers, California, earthquake. *Science*, **260**, 1617–1623, http://doi.org/10.1126/science.260.5114.1617

Hill, D.P., Pollitz, F. & Newhall, C. 2002. Earthquake–volcano interactions. *Physics Today*, **55**, 41–47.

Jaggar, T.A., Finch, R.H. & Emerson, O.H. 1924. The lava tide, seasonal tilt, and the volcanic cycle. *Monthly Weather Review*, **52**, 142–145.

Jones, J.P., Carniel, R. & Malone, S.D. 2012. Decomposition, location, and persistence of seismic signals recovered from continuous tremor at Erta 'Ale, Ethiopia. *Journal of Volcanology and Geothermal Research*, **213**, 116–129, http://doi.org/10.1016/j.jvolgeores.2011.07.007

Jónsson, S. & Xu, W. 2015. Volcanic eruptions in the Southern Red Sea during 2007–2013. *In*: Rasul, N.M.A. & Stewart, I.C.F. (eds) *The Red Sea*. Springer, Berlin, 175–186.

Jónsson, S., Zebker, H., Segall, P. & Amelung, F. 2002. Fault slip distribution of the 1999 MW 7.1 Hector Min, California, earthquake, estimated from satellite radar and GPS measurements. *Bulletin of the Seismological Society of America*, **92**, 1377–1389, http://doi.org/10.1785/0120000922

Justice, C.O., Vermote, E. *et al.* 1998. The Moderate Resolution Imaging Spectroradiometer (MODIS): land remote sensing for global change research. *IEEE Transactions on Geoscience and Remote Sensing*, **36**, 1228–1249, http://doi.org/10.1109/36.701075

Justice, C.O., Townshend, J.R.G. *et al.* 2002. An overview of MODIS Land data processing and product status. *Remote Sensing of Environment*, **83**, 3–15, http://doi.org/10.1016/s0034-4257(02)00084-6

Justice, C.O., Giglio, L., Boschetti, L., Roy, D., Csiszar, I., Morisette, J. & Kaufman, Y. 2006. Algorithm Technical Background Document: MODIS Fire Products, http://modis-fire.umd.edu/files/atbd_mod14.pdf

Kaufman, Y.J., Justice, C.O. *et al.* 1998. Potential global fire monitoring from EOS-MODIS. *Journal of Geophysical Research*, **103**, 32215–32238, http://doi.org/10.1029/98jd01644

Keir, D., Hamling, I.J. *et al.* 2009. Evidence for focused magmatic accretion at segment centers from lateral dike injections captured beneath the Red Sea rift in Afar. *Geology*, **37**, 59–62.

La Femina, P.C., Connor, C.B., Hill, B.E., Strauch, W. & Saballos, J.A. 2004. Magma–tectonic interactions in Nicaragua: the 1999 seismic swarm and eruption of Cerro Negro volcano. *Journal of Volcanology and Geothermal Research*, **137**, 187–199, http://doi.org/10.1016/j.jvolgeores.2004.05.006

Le Guern, F., Carbonnelle, J. & Tazieff, H. 1979. Erta 'Ale lava lake – heat and gas transfer to the atmosphere. *Journal of Volcanology and Geothermal Research*, **6**, 27–48.

Linde, A.T. & Sacks, I.S. 1998. Triggering of volcanic eruptions. *Nature*, **395**, 888–890.

Manga, M. & Brodsky, E. 2006. Seismic triggering of eruptions in the far field: volcanoes and geysers. *Annual Review of Earth and Planetary Sciences*, **34**, 263–291.

Marchese, F., Filizzola, C., Mazzeo, G., Paciello, R., Pergola, N. & Tramutoli, V. 2009. Robust satellite techniques for thermal volcanic activity monitoring, early warning and possible prediction of new eruptive events. *In*: *Geoscience and Remote Sensing Symposium, 2009 IEEE International, IGARSS 2009*, 12–17 July, Cape Town, II-953–II-956, http://doi.org/10.1109/IGARSS.2009.5418258

Markham, B.L., Stovey, J.C., Williams, D.L. & Irons, J.R. 2004. Landsat sensor performance: history and

current status. *IEEE Transactions on Geoscience and Remote Sensing*, **42**, 2691–2694, http://doi.org/10.1109/TGRS.2004.840720

Mohr, P. 1962. The Ethiopian rift system. *Bulletin of the Geophysical Observatory of Addis Ababa*, **5**, 33–62.

Müller, J. 2010. MSG Level 1.5 Image Data Format Description. EUM/MSG/ICD/105. EUMETSAT, Germany, https://www.eumetsat.int/website/wcm/idc/idcplg?IdcService=GET_FILE&dDocName=PDF_TEN_05105_MSG_IMG_DATA&RevisionSelectionMethod=LatestReleased&Rendition=Web

Murphy, S.W., Wright, R., Oppenheimer, C. & Filho, C.R.S. 2013. MODIS and ASTER synergy for characterizing thermal volcanic activity. *Remote Sensing of Environment*, **131**, 195–205, http://doi.org/10.1016/j.rse.2012.12.005

Neuberg, J. 2000. External modulation of volcanic activity. *Geophysical Journal International*, **142**, 232–240, http://doi.org/10.1046/j.1365-246x.2000.00161.x

Nobile, A., Pagli, C., Keir, D., Wright, T.J., Ayele, A., Ruch, J. & Acocella, V. 2012. Dike-fault interaction during the 2004 Dallol intrusion at the northern edge of the Erta 'Ale Ridge (Afar, Ethiopia). *Geophysical Research Letters*, **39**, L19305, http://doi.org/10.1029/2012gl053152

Oppenheimer, C. & Francis, P. 1997. Remote sensing of heat, lava and fumarole emissions from Erta 'Ale volcano, Ethiopia. *International Journal of Remote Sensing*, **18**, 1661–1692.

Oppenheimer, C. & Francis, P. 1998. Implications of longeval lava lakes for geomorphological and plutonic processes at Erta 'Ale volcano, Afar. *Journal of Volcanology and Geothermal Research*, **80**, 101–111.

Oppenheimer, C. & Yirgu, G. 2002. Thermal imaging of an active lava lake: Erta 'Ale volcano, Ethiopia. *International Journal of Remote Sensing*, **23**, 4777–4782, http://doi.org/10.1080/01431160110114637

Oppenheimer, C., McGonigle, A.J.S., Allard, P., Wooster, M.J. & Tsanev, V. 2004. Sulfur, heat, and magma budget of Erta 'Ale lava lake, Ethiopia. *Geology*, **32**, 509–512, http://doi.org/10.1130/g20281.1

Pagli, C., Wright, T.J., Ebinger, C.J., Yun, S.-H., Cann, J.R., Barnie, T. & Ayele, A. 2012. Shallow axial magma chamber at the slow-spreading Erta 'Ale Ridge. *Nature Geoscience*, **5**, 284–288.

Pagli, C., Wang, H., Wright, T.J., Calais, E. & Lewi, E. 2014. Current plate boundary deformation of the Afar rift from a 3-D velocity field inversion of InSAR and GPS. *Journal of Geophysical Research*, **119**, 8562–8575, http://doi.org/10.1002/2014JB011391

Palmieri, L. 1873. Indagini spettroscopiche sulle sublimazioni vesuviane. *Rendiconto dell' Accademia delle scienze fisiche e matematiche, Serie I*, **12**, 31–44.

Peters, N., Oppenheimer, C., Killingsworth, D.R., Frechette, J. & Kyle, P. 2014. Correlation of cycles in Lava Lake motion and degassing at Erebus Volcano, Antarctica. *Geochemistry, Geophysics, Geosystems*, **15**, 3244–3257, http://doi.org/10.1002/2014gc00 5399

Powell, S.L., Pflugmacher, D., Kirschbaum, A.A., Kim, Y. & Cohen, W.B. 2007. Moderate resolution remote sensing alternatives: a review of Landsat-like sensors and their applications. *Journal of Applied Remote Sensing*, **1**, http://doi.org/10.1117/1.2819342

Rosen, P.A., Hensley, S., Peltzer, G. & Simons, M. 2004. Updated repeat orbit interferometry package released. *Eos, Transactions of the AGU*, **85**, 47–47, http://doi.org/10.1029/2004eo050004

Sawyer, G.M., Oppenheimer, C., Tsanev, V.I. & Yirgu, G. 2008. Magmatic degassing at Erta 'Ale volcano, Ethiopia. *Journal of Volcanology and Geothermal Research*, **178**, 837–846, http://doi.org/10.1016/j.jvolgeores.2008.09.017

Shimozuru, D. 1975. Lava lake oscillations and the magma reservoir beneath a volcano. *Bulletin Volcanologique*, **39**, 570–580, http://doi.org/10.1007/bf02596977

Shimozuru, D. 1987. Tidal effects on Hawaiian volcanism. *In*: Decker, R.W., Wright, T.L. & Stauffer, P.H. (eds) *Volcanism in Hawaii*. US Geological Survey Professional Paper, **1350**, 1337–1344.

Shuler, A. & Nettles, M. 2012. Earthquake source parameters for the 2010 western Gulf of Aden rifting episode. *Geophysical Journal International*, **190**, 1111–1122, http://doi.org/10.1111/j.1365-246X.2012.05529.x

Sottili, G. & Palladino, D.M. 2012. Tidal modulation of eruptive activity at open-vent volcanoes: evidence from Stromboli, Italy. *Terra Nova*, **24**, 233–237, http://doi.org/10.1111/j.1365-3121.2012.01059.x

Spampinato, L., Oppenheimer, C., Calvari, S., Cannata, A. & Montalto, P. 2008. Lava lake surface characterization by thermal imaging: Erta 'Ale volcano (Ethiopia). *Geochemistry, Geophysics, Geosystems*, **9**, Q12008, http://doi.org/10.1029/2008gc002164

Spampinato, L., Ganci, G. *et al.* 2013. Thermal insights into the dynamics of Nyiragongo lava lake from ground and satellite measurements. *Journal of Geophysical Research Solid Earth*, **118**, 5771–5784, http://doi.org/10.1002/2013jb010520

Tazieff, H. 1973. Erta 'Ale volcano. *Revue de géographie physique et de géologie dynamique*, **15**, 437–43.

Ungar, S.G., Pearlman, J.S., Mendenhall, J.A. & Reuter, D. 2003. Overview of the Earth Observing One (EO-1) mission. *IEEE Transactions on Geoscience and Remote Sensing*, **41**, 1149–1159, http://doi.org/10.1109/tgrs.2003.815999

Varet, J. 1971. Recent activity of Erta (Dankalie, Ethiopie). *Comptes rendus hebdomadaires des seances de l'Academie des sciences serie D*, **272**, 1964.

Volcano Discovery 2015. http://www.volcanodiscovery.com/

Wadge, G. 1981. The variation of magma discharge during basaltic eruptions. *Journal of Volcanology and Geothermal Research*, **11**, 139–168, http://doi.org/10.1016/0377-0273(81)90020-2

Walter, T.R. 2007. How a tectonic earthquake may wake up volcanoes: stress transfer during the 1996 earthquake–eruption sequence at the Karymsky Volcanic Group, Kamchatka. *Earth and Planetary Science Letters*, **264**, 347–359, http://doi.org/10.1016/j.epsl.2007.09.006

Walter, T.R. & Amelung, F. 2007. Volcanic eruptions following M $\geq$ 9 megathrust earthquakes: implications for the Sumatra-Andaman volcanoes. *Geology*, **35**, 539–542, http://doi.org/10.1130/g23429a.1

WANG, H., WRIGHT, T.J., YU, Y., LIN, H., JIANG, L., LI, C. & QIU, G. 2012. InSAR reveals coastal subsidence in the Pearl River Delta, China. *Geophysics Journal International*, **191**, 1119–1128, http://doi.org/10.1111/j.1365-246X.2012.05687.x

WRIGHT, R. & PILGER, E. 2008. Satellite observations reveal little inter-annual variability in the radiant flux from the Mount Erebus lava lake. *Journal of Volcanology and Geothermal Research*, **177**, 687–694, http://doi.org/10.1016/j.jvolgeores.2008.03.005

WRIGHT, R., FLYNN, L.P., GARBEIL, H., HARRIS, A.J. & PILGER, E. 2004. MODVOLC: near-real-time thermal monitoring of global volcanism. *Journal of Volcanology and Geothermal Research*, **135**, 29–49, http://doi.org/10.1016/j.jvolgeores.2003.12.008

WRIGHT, T.J., EBINGER, C., BIGGS, J., AYELE, A., YIRGU, G., KEIR, D. & STORK, A. 2006. Magma-maintained rift segmentation at continental rupture in the 2005 Afar dyking episode. *Nature*, **442**, 291–294.

XU, W. & JÓNSSON, S. 2014. The 2007–8 volcanic eruption on Jebel at Tair island (Red Sea) observed by satellite radar and optical images. *Bulletin of Volcanology*, **76**, 1–14.